ORIGINAL RESEARCH

Characterizing the Oxygen Minimum Zone (OMZ) in the Costa Rican Eastern Tropical Pacific using *in situ* data from field campaigns

Alejandro Rodríguez[1, 2, 3], Eric J. Alfaro[1, 2, 3, *] and Jorge Cortés[1, 4]

[1]Centro de Investigación en Ciencias del Mar y Limnología (CIMAR), Ciudad de la Investigación, Universidad de Costa Rica (UCR), 11501-2060 - San José, Costa Rica. [2]Escuela de Física, Sede Rodrigo Facio, Universidad de Costa Rica (UCR), 11501-2060 - San José, Costa Rica. [3]Centro de Investigaciones Geofísicas (CIGEFI), Ciudad de la Investigación, Universidad de Costa Rica (UCR), 11501-2060 - San José, Costa Rica. [4]Escuela de Biología, Sede Rodrigo Facio, Universidad de Costa Rica (UCR), 11501-2060 - San José, Costa Rica. ORCID *Alejandro Rodríguez* https://orcid.org/0000-0003-4618-6560, *Eric J. Alfaro* https://orcid.org/0000-0001-9278-5017, *Jorge Cortés* https://orcid.org/0000-0001-7004-8649

Marine and Fishery Sciences MAFIS

ABSTRACT. For conservation and sustainable fisheries, it is important to characterize the Oxygen Minimum Zones or OMZ in and around the methane seeps of the Eastern Tropical Pacific (ETP), Costa Rica, through the analysis of temperature, salinity, density, and oxygen profiles. The data used in this work were collected during several oceanographic research campaigns in the Pacific continental margin and offshore of Costa Rica, between 2009 and 2019, using a CTDs, as the profiler of physical parameters of the water column. In general, it was observed that dissolved oxygen gradually decreases with depth to the thermocline, then its concentration decreases more rapidly and remains low, indicating the presence of the OMZ and tends to increase slightly at greater depths. Mean vertical extension of the OMZ near and around the seeps was 763 m and the mean depth for the minimum dissolved oxygen value was 393 m. Spatial differences of measurements taken at stations near the methane seeps were calculated with respect to the measurements at the station located above them. Overall, a greater variability of the oxygen anomalies was observed within the mixed layer, while under the thermocline their values remain stable and around zero.

Key words: Anoxia, international collaboration, Central America, methane seeps, continental margin, CTD profiles.

*Correspondence:
erick.alfaro@ucr.ac.cr

Received: 2 June 2023
Accepted: 15 January 2024

ISSN 2683-7595 (print)
ISSN 2683-7951 (online)

https://ojs.inidep.edu.ar

Journal of the Instituto Nacional de Investigación y Desarrollo Pesquero (INIDEP)

Caracterización de la Zona Mínima de Oxígeno en el Pacífico Tropical Oriental costarricense utilizando datos *in situ* de campañas de campo

RESUMEN. Para la conservación y la pesca sostenible, es importante caracterizar las Zonas de Mínimo de Oxígeno o ZMO en y alrededor de las filtraciones de metano del Pacífico Tropical Oriental, Costa Rica, mediante el análisis de perfiles de temperatura, salinidad, densidad y oxígeno. Los datos utilizados en este trabajo fueron recolectados durante diferentes campañas de investigación oceanográfica en el margen continental del Pacífico de Costa Rica, entre 2009 y 2019, utilizando un CTD, como perfilador de parámetros físicos de la columna de agua. En general, se observó que el oxígeno disuelto disminuye gradualmente con la profundidad hasta la termoclina, luego su concentración disminuye más rápidamente y permanece baja, indicando la presencia de la OMZ y tiende a aumentar ligeramente a mayores profundidades. La extensión vertical media de la OMZ cerca y alrededor de las filtraciones fue de 763 m y la profundidad media del valor mínimo de oxígeno disuelto fue de 393 m. Se calcularon las diferencias espaciales de las mediciones realizadas en las estaciones cercanas a las filtraciones de metano con respecto a las mediciones en la estación ubicada sobre ellas. En términos generales, se observó una mayor variabilidad de las anomalías de oxígeno dentro de la capa de mezcla, mientras que bajo la termoclina sus valores se mantienen estables y alrededor de cero.

Palabras clave: Anoxia, colaboración internacional, América Central, filtraciones de metano, márgenes continentales, perfiles de CTD.

INTRODUCTION

The interaction between the atmosphere and the ocean allows oxygen transfer from the atmosphere to the surface layers of the ocean by diffusion and to the deeper layers by circulation of oxygenated surface water (Levin 2002). Water masses at intermediate depths are classified as Oxygen Minimum Zones (OMZs) when oxygen concentrations are low (hypoxia) or null (anoxia) (Rixen et al. 2020; Kirchman 2021). OMZs are caused by high biological consumption and the effects of strong thermal stratification on ventilation (Fiedler and Talley 2006; Karstensen et al. 2008; Gooday et al. 2010; Cabré et al. 2015). Stratification restricts vertical mixing and upwelling as it separates water masses by age, where older water bodies have lower oxygen concentrations (Rixen et al. 2020). High primary production and the resultant increase in organic matter transport to intermediate depths affect the intensity of the OMZs since oxygen consumption is enhanced by decomposition of organic matter (Levin 2002; Matear and Hirst 2003; Dale et al. 2015). Therefore, a decrease in primary productivity reduces the export of organic matter to intermediate depths, resulting in lower oxygen consumption (Sarma et al. 2020). Low oxygen concentrations suppress the consumption of organic matter, preventing further oxygen depletion in the surface layers and allowing unconsumed organic matter to sink to the bottom (Rixen et al. 2020). Organic matter consumption is favored by slower sink rates that result in increased deoxygenation and thickening of the OMZ (Sarma et al. 2020). As a result, the respiration of the exported organic matter is favored at the bottom of the OMZ, intensifying deoxygenation and pushing the lower boundary of the OMZ deeper (Rixen et al. 2020). The intensity of eddy activity could also influence oxygen levels, as oxygen injection through eddy pumping weakens the OMZs (Rixen et al. 2020; Sarma et al. 2020).

There is no consensus on the definition of the limits of the OMZ despite its importance in improving the understanding of their location, characteristics, and biogeochemical effects (Trucco-Pignata et al. 2019; Kirchman 2021). The OMZ definition/limits are usually defined as a function of O_2 concentration among different classifications. For the present study, the OMZ was defined by a dissolved oxygen concentration of 0.5 ml l^{-1}, equivalent to 22 µM or 20 µmol kg^{-1} (Levin 2003; Helly and Levin 2004; Karstensen et al. 2008; Gooday et al. 2010). In addition, Karstensen et al. (2008) specified three different thresholds: 0.1 ml l^{-1} or 4.5 µmol kg^{-1} for the suboxic level, a more rigid level defined as 45 µmol kg^{-1}, and a more relaxed level at 90 µmol kg^{-1}.

According to sedimentary records, the OMZs can remain through millennia and extend for thousands of kilometers in open oceans with high productivity or in the eastern edges of ocean basins where the spatial and temporal variability is higher (Levin 2002; Gooday et al. 2010; Loescher et al. 2016; Rixen et al. 2020). Off the western continental coasts, where wind-driven currents and the Coriolis effect replace surface waters with cold nutrient-rich waters, primary productivity thrives and generates excessive organic matter that is decomposed by bacteria with the consumption of oxygen giving rise to an OMZ when conditions persist over time (Levin 2002). The minimal oxygen and light conditions of an OMZ lead to accumulation of organic matter due to the sluggish decomposition. The enhanced respiration of organic matter results in acidic conditions, pH values between 7.7 and 7.8

in the core of the OMZ were observed in the Eastern Tropical Pacific (ETP) off Costa Rica (Gooday et al. 2010). The biodiversity in the OMZs depends on the oxygen and organic matter concentrations (Neira et al. 2018). OMZ waters are characterized by low diversity, with the lack of mobile microorganisms, but the waters in the lowest limit present an increase in biological productivity (Stramma et al. 2008; Gooday et al. 2010). In anoxic waters, hydrogen sulfide is usually observed due to the null concentrations of oxygen (Rixen et al. 2020).

The ETP in Mesoamerica is a region with atmosphere and ocean features that interacts through its interface. Among those features are the Mid-Summer Drought, a relative minimum observed in the precipitation between June and September (Amador et al. 2016a, 2016b; Durán-Quesada et al. 2020; García-Franco et al. 2023), and two important upwelling systems. The first one is the seasonal coastal regions located in the Gulfs of Tehuantepec, Papagayo and Panama, observed mainly in the boreal winter (Alfaro and Lizano 2001; Amador et al. 2016a, 2016b; Durán-Quesada et al. 2020; Escoto-Murillo and Alfaro 2021; Rodríguez et al. 2021) and the second one is the Costa Rica Thermal Dome (Alfaro and Lizano 2001; Amador et al. 2016a, 2016b; Lizano 2016; Ross-Salazar et al. 2019; Duran-Quesada et al. 2020). Those upwelling systems have some interactions mainly during the winter and during the Mid-Summer Drought occurrence in July-August. Comprehensive studies about the characteristics of a variety of atmospheric and oceanic systems dominated by multiscale interaction processes in the ETP, reviewing the climate and climate variability are presented in Amador et al. (2016a, 2016b).

Additionally, two of the best studied, most intense, and largest OMZs in the world are located in the ETP, separated by the Equatorial Undercurrent (EUC), which in addition to the Northern and Southern Equatorial Countercurrent (ECC), Subsurface Countercurrent (SCC), and Intermediate Countercurrent (ICC) conform the eastward tropical currents which transport relatively oxygen-rich water to the ETP (Stramma et al. 2008, 2010; Cabré et al. 2015). The upwelling systems mentioned previously are important for the ETP OMZ since vertical displacement of water masses alters oxygen concentrations as deep-water upwelling brings nutrients to the surface, increasing biological productivity and the subsequent consumption of oxygen, while the descent of surface water masses counteracts productivity and injects oxygen into intermediate depths (Gruber et al. 2011; Rixen et al. 2020). Moreover, a faster circulation of the water allows the supply of oxygen to the deeper layers of the ocean, thus influencing the intensity of the OMZs (Sarma et al. 2020). There are OMZs also in the Atlantic, favored by the high productivity observed in both oceans because of the current upwelling systems in the eastern continental shelves and in the northern reaches of the tropical Indian Ocean, home to about a fifth of the ocean's oxygen depleted areas, where the upwelling is associated with the monsoon (Levin 2002; Stramma et al. 2008; Rixen et al. 2020).

The expansion and intensification of the OMZ added to eutrophication can cause negative repercussions such as changes in benthic and pelagic ecosystems, decreases in marine biodiversity, disturbances in food chains, primary production, populations, fishery yield, biogeochemical processes, and more frequent sulfur events, as a consequence of the dependence of nutrient budgets, biological productivity, and carbon fixation on dissolved oxygen concentrations (Levin 2002; Stramma et al. 2008; Gooday et al. 2010; Fee 2012; Loescher et al. 2016; Breitburg et al. 2018; Rixen et al. 2020).

The Costa Rica Thermal Dome (Lizano 2016; Ross-Salazar et al. 2019) corresponds to the northern OMZ and is characterized by a more intense deoxygenation and a larger and thicker extension than the southern OMZ, due to differences in oxygen income and a low oxygen core around 500 m (Stramma et al. 2010; Cabré et al. 2015). The vertical extents of the OMZs in the ETP range from around 100 m to 900 m (Karstensen et al. 2008). The OMZs in the ETP are caused by upwelling effects, sluggish horizontal transport, high primary productivity, and stratification driven primarily by temperature (Karstensen et al. 2008; Fiedler et al. 2013). In addition to this North-South pattern, the intensity and extent of the OMZs in the area tend to increase towards the east and are affected by the concentration of nutrients and oxygen, among other properties of the water source (Stramma et al. 2010).

The OMZs in the ETP do not present strong seasonal variability (Paulmier and Ruiz-Pino 2009). However, El Niño-Southern Oscillation (ENSO) and the Pacific Decadal Oscillation (PDO) are sources of interannual and decadal variability in the ETP (Durán-Quesada et al. 2020) influencing on the OMZs variability (Stramma et al. 2010; Czeschel et al. 2012). ENSO events can alter dissolved oxygen concentrations in OMZs through physical and biogeochemical processes that affect biological productivity above the OMZ, ventilation, and thermocline and oxycline depths (Espinoza-Morriberón et al. 2019). Equatorial Kelvin waves can deepen the thermocline and oxycline in the ETP during El Niño, the ENSO warm phase (Enfield 1987; Alfaro y Lizano 2001; Fuenzalida et al. 2009; Stramma et al. 2010; Escoto-Murillo and Alfaro 2021). As regards the PDO, it alters dissolved oxygen through isopycnal (‘heave’) in tropical waters and by subduction in subtropical waters (Ito et al. 2019). According to a study by Duteil et al. (2018), oxygen in the ETP decreases during a transition from the negative to the positive multi-decadal PDO.

Water masses from different oxygen-rich sources can be found in the ETP, as is the case of the Tropical Surface Water (TSW), located above the OMZs and characterized by warm temperatures and low salinities with values above 25 °C and below 34 respectively, the Subtropical Subsurface Water (SSW), also known as Subtropical Underwater (STUW), a high salinity water identified by its subsuperficial salinity maximum with temperatures around 13 °C and salinities above 34.9, transported eastward by the EUC, and Antarctic Intermediate Water (AAIW), identified by its characteristic salinity minimum of 34.55 and cold temperatures under 5 °C, transported eastward by the Southern and Northern SCC and ICC (Wyrtki 1967; Brenes and Coen 1985; Fiedler and Talley 2006; Stramma et al. 2010). According to Mora-Escalante et al. (2020) TSW above 50 m depth and SSW below 60 m depth were observed in the ETP from CTD profiles sampled in the region between 2008 and 2012.

Previous paragraphs state that OMZs are often areas with depressed marine life due to the very low concentration of oxygen. However, specialized microorganisms can thrive in these ecosystems being important regions for biogeochemical process in the ocean, mainly nitrogen and carbon. For this reason, the study of OMZ is important not only to the nutrient cycles, but also to understand the diversity and adaptation of life in this extreme environment. OMZs can be altered by various environmental factors, such as ocean temperature, circulation, upwelling and acidification among others, and so climate change could have significant implications on OMZs. This study has a significant dataset of oceanographic campaigns totaling around 10 years of data in the Eastern Tropical Pacific off Costa Rica (but not continuous measurements) which could be relevant to characterize variations of the OMZ of this region. Furthermore, it was based on the analysis of oceanographic data measured with CTD profilers at hydrographic stations in the ETP during five different scientific campaigns carried out between 2009 and 2019. Besides Brenes et al. (2016) and Mora-Escalante et al. (2020), this is one of the first studies to focus on the analysis of data obtained from *in situ* measurements of the study region.

MATERIALS AND METHODS

Study area and sampling campaigns

An oceanographic database composed by the cast profiles of the water column of the hydrographic stations sampled during five scientific campaigns carried out in the ETP of Costa Rica between 2009 and 2019 was compiled. The AT15-44 (from February 21 to March 8, 2009), AT15-59 (from January 6 to 13, 2010), and AT37-13 (from May 20 to June 11, 2017) campaigns were carried out onboard the research vessel RV 'Atlantis'. The JC112 campaign from December 5, 2014, to January 16, 2015, was carried out by the RRS 'James Cook'. The FK190106 campaign from January 6 to 27, 2019, was developed by the RV 'Falkor'. In every campaign, the hydrographic stations were profiled with a Sea-Bird SBE 911+ CTD. In the campaigns of the RV 'Atlantis' a Sea-Bird SBE 19 CTD installed in the HOV 'Alvin' was also used. Samplings were carried out at several hydrographic stations distributed within the ETP of Costa Rica, with a special focus on stations located approximately above the methane seeps at 8.93° N and 84.31° W (Central stations) and in the surroundings of the seeps to the northeast (NE station) at 9.02° N and 84.20° W, to the southeast (SE station) at 8.85° N and 84.22° W, to the southwest (SW station) at 8.87° N and 84.43° W, and to the northwest (NW station) at 9.02° N and 84.41° W (Figure 1), with maximum depths between 391 m and 3,272 m. The latitude, longitude and date of all casts used in this work are included in Tables A1-A4 of the Appendix. This ecosystem found in the hydrothermal or methane seeps is described in detail by Levin et al. (2012).

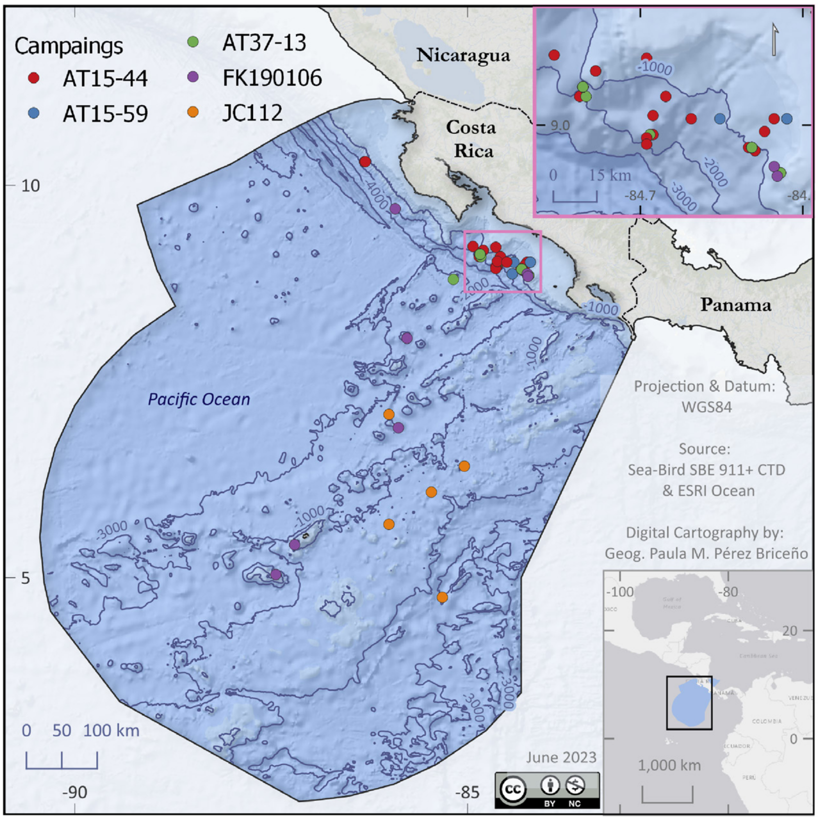

Figure 1. Location of the CTD casts used. Red dots are AT15-44, blue for AT15-59, green for AT37-13, purple for FK190106 and orange for JC112 campaigns, respectively. Light blue area in the map represent the Pacific Costa Rican exclusive economic zone.

Data analysis

Raw data were retrieved from online databases or provided by researchers associated with the campaigns. Data were processed with the SBE Data Processing software of Sea-Bird Electronics, which was used to convert the raw data to engineering units, resolve measurement inaccuracies due to sensors, remove inaccurate values, calculate the derived variables, average the data every meter of depth, export data in ASCII format, and plot preliminary profiles of the variables. The derived variables that were calculated are depth, seawater density, and practical salinity (Sea-Bird Electronics 2016). Dissolved oxygen concentrations were obtained from measurements of a sensor that counts the number of oxygen molecules per second through a polarographic membrane (Sea-Bird Electronics 2013). Dissolved oxygen data from 47 casts were obtained only from the samplings carried out with Sea-Bird SBE 911+ CTD profilers, since these had the required sensor.

Scripts for further data processing and visualization were programmed in Python with Jupyter Notebook (Van Rossum and Drake 2009). Maps with the locations of the hydrographic stations were plotted (e.g. Figure 1). For every campaign, all the casts done at the Central station, over the hydrothermal vents, were averaged. Spatial anomalies in the vicinity of the hydrothermal or methane seeps vents were obtained from the differences of the samplings of each neighboring station (NE, SE, SW, and NW) with respect to the averages of the Central station, by variable and campaign. Anomalies between the averages of the Central station, from data sampled by the HOV 'Alvin' CTD, and the averages of the Central station, from data measured by the RV 'Atlantis' CTD, by variable and campaign, were also obtained. Tables compile maximum and minimum values of each variable, maximum gradients, vertical extension and upper and lower boundaries of the water masses and of the OMZ, descriptive statistics, latitude, longitude and date of samplings. The oxygen values in the tables have four significant numbers so that their variability can be better appreciated. The profiles of the samplings, averages, and anomalies were plotted, by variable, station, and campaign. The T-S diagrams of the averages of the Central station over the methane seeps were plotted by CTD profiler and campaign.

RESULTS

Regarding the five hydrographic stations closest to the methane seeps, the AT15-59 campaign included samplings with the CTD of the RV 'Atlantis' at the Central, NE, SE, SW, and NW stations, the AT15-44 campaign at the Central, NE, SE, and SW stations, and the AT37-13 campaign at the Central and SE stations. During the three campaigns of the RV 'Atlantis', samplings were also carried out with the CTD of the HOV 'Alvin' at the Central station. As for sampling averages in the Central station for the three campaigns, it was found that the temperature decreases rapidly within the mixed layer and more gradually at greater depths (Figure 2). Salinity increases with depth in shallow waters, peaks at the salinity subsurface maximum and then decreases slightly, stabilizing at greater depths. Density also surges with depth with a higher rate of change within the mixed layer. Dissolved oxygen decreases with depth up to the upper limit of the OMZ, decreases slower up to the core of the OMZ and then increases slightly with depth (Figure 2).

With respect to the data measured with the HOV 'Alvin' CTD, the variables show a trend similar to that observed in the profiles obtained from the samplings with the RV 'Atlantis' CTD (Figure 3; Tables 1 and 2).

Anomalies of data sampled in stations in the surroundings with respect to the averages of the data measured in the Central station, for the different campaigns, generally oscillate with greater amplitude in the mixed layer, while under the thermocline they remain stable and tend to zero. Particu-

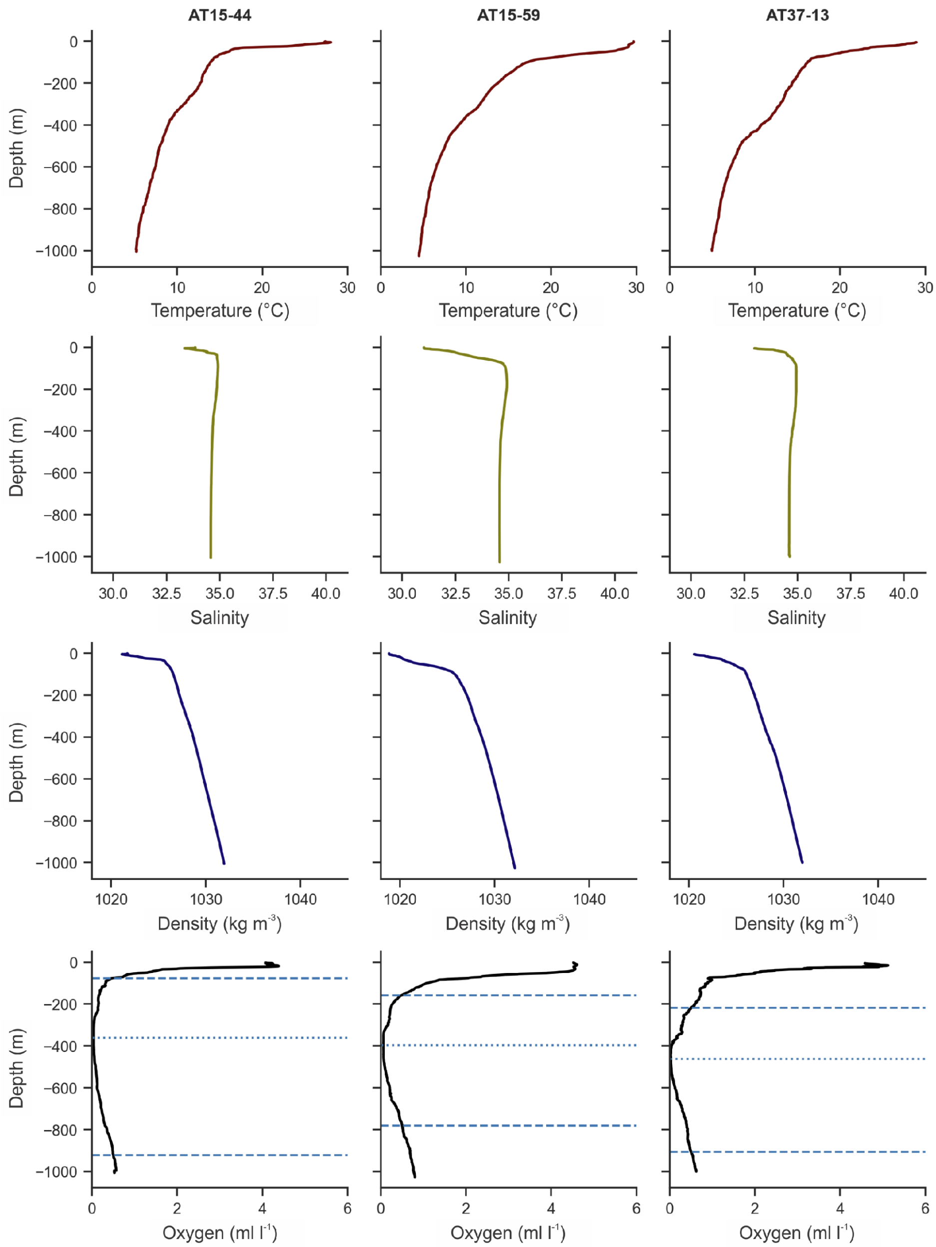

Figure 2. Averages of temperature, salinity, density, and oxygen, at the Central station, from data measured by the RV 'Atlantis' CTD profiler during the AT15-44 (2009), AT15-59 (2010), and AT37-13 (2017) campaigns. In the oxygen profiles, the horizontal dashed lines represent the upper and lower boundaries of the OMZ (dissolved oxygen < 0.5 ml l^{-1}), and the horizontal dotted lines indicate the minimum oxygen.

larly, in the profiles corresponding to the AT15-44 campaign, within the mixed layer, positive anomalies of temperature and oxygen stand out in the SE station and negative anomalies of temperature in NE and SW, salinity in NE, SE, and SW, density in SE, and oxygen in NE and SW (Figure 4). Re-

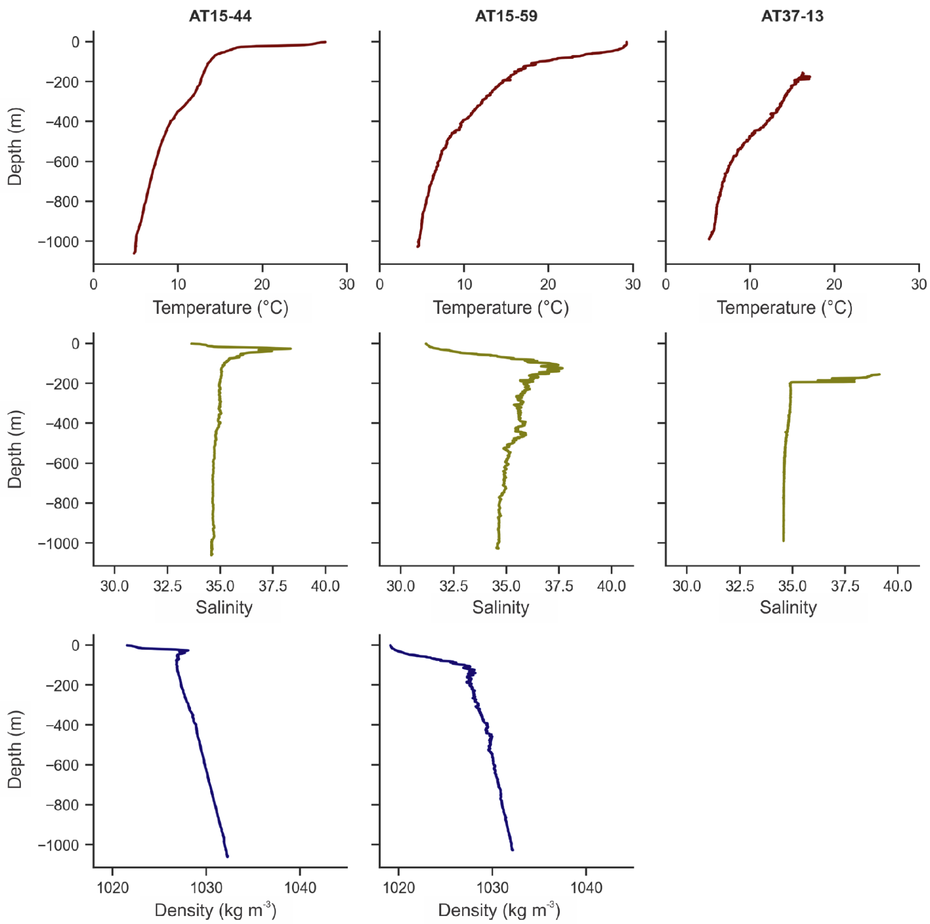

Figure 3. Averages of temperature, salinity, and density, at the Central station, from data measured by the HOV Alvin CTD profiler during the AT15-44, AT15-59, and AT37-13 campaigns.

garding the AT15-59 campaign, positive anomalies of salinity within the mixed layer were observed in stations SE, SW, and NW, density in SE and NW, and oxygen in SW, while negative anomalies of temperature in NW, salinity in NE and oxygen in SE and NW (Figure 5). Under the thermocline the temperature anomaly in the NE and SW stations oscillates mainly within a negative range and in the SE station in a positive range. With respect to the AT37-13 campaign, in the profiles of the SE station it is observed that negative salinity, density, and oxygen anomalies prevail in the mixed layer and positive temperature anomalies stand out under the thermocline (see rigth column of Figure 4).

Anomalies of averages of variables sampled in the Central station by the HOV 'Alvin' CTD with respect to the averages of the variables sampled in the Central station by the RV 'Atlantis' CTD follow a similar pattern, since profiles in Figure A1 show important oscillations within the mixing layer and tend to zero below it. In particular, profiles of the AT15-44 campaign exhibit the temperature anomaly tends to the negative axis and the salinity and density anomalies to the positive axis, within the mixed layer, while below it anomalies of the three variables remain stable with values closer to zero. Regarding profiles corresponding to the AT15-59 campaign, the three variables were very similar

Table 1. Maximum and minimum values of the averages of temperature and salinity, for the Central, NE, SE, SW, and NW stations, from data measured by the RV 'Atlantis' CTD and HOV 'Alvin' CTD profilers during the AT15-44, AT15-59, and AT37-13 campaigns, with their respective depth and station ID.

		Temperature (°C)	Depth (m)	ID	Salinity	Depth (m)	ID
Central	Max.	29.98	5	AT15-59-1	34.98	116	AT37-13-2
	Min.	4.47	1,025	AT15-59-8	30.79	1	AT15-59-3
NE	Max.	29.91	4	AT15-59-2	34.92	72	AT15-44-2
	Min.	8.15	437	AT15-44-2	29.99	2	AT15-59-2
SE	Max.	29.37	2	AT15-59-4	34.97	124	AT37-13-5
	Min.	9.23	393	AT15-59-4	31.07	1	AT15-59-4
SW	Max.	29.34	1	AT15-59-6	34.93	142	AT15-59-6
	Min.	2.49	1,811	AT15-59-6	31.33	1	AT15-59-6
NW	Max.	29.71	2	AT15-59-9	34.93	157	AT15-59-9
	Min.	4.02	1,155	AT15-59-9	31.09	2	AT15-59-9
'Alvin'	Max.	29.79	2	AT37-13-4909	40.71	27	AT15-44-4501
	Min.	2.07	2,228	AT15-44-4507	30.82	3	AT15-59-4587

Table 2. Maximum and minimum values of the averages of density and oxygen, for the Central, NE, SE, SW, and NW stations, from data measured by the RV 'Atlantis' CTD and HOV 'Alvin' CTD profilers during the AT15-44, AT15-59, and AT37-13 campaigns, with their respective depth and station ID.

		Density (kg m^{-3})	Depth (m)	ID	Oxygen (ml l^{-1})	Depth (m)	ID
Central	Max.	1,032.16	1,027	AT15-59-8	5.2268	15	AT37-13-1
	Min.	1,018.62	1	AT15-59-1	0.0177	444	AT37-13-1
NE	Max.	1,028.96	437	AT15-44-2	4.6523	8	AT15-59-2
	Min.	1,018.01	2	AT15-59-2	0.0394	331	AT15-44-2
SE	Max.	1,028.62	394	AT15-59-4	4.6777	26	AT15-44-14
	Min.	1,019.00	1	AT15-59-4	0.0393	369	AT15-44-14
SW	Max.	1,036.06	1,815	AT15-44-5	4.6064	9	AT15-59-6
	Min.	1,019.21	1	AT15-59-6	0.0388	324	AT15-44-5
NW	Max.	1,032.82	1,155	AT15-59-9	4.6216	6	AT15-59-9
	Min.	1,018.90	2	AT15-59-9	0.0576	477	AT15-59-9
'Alvin'	Max.	1,038.05	2,225	AT15-44-4507			
	Min.	1,018.84	2	AT15-59-4587			

and they keep the same trend along the water column, and the profile of the salinity anomaly for the AT37-13 campaign remains more stable and nearer to zero under the mixed layer.

There were three distinguishable water masses in the T-S diagrams of sampling averages over the hydrothermal vents at the Central station for CTD profilers used during the three campaigns of the RV

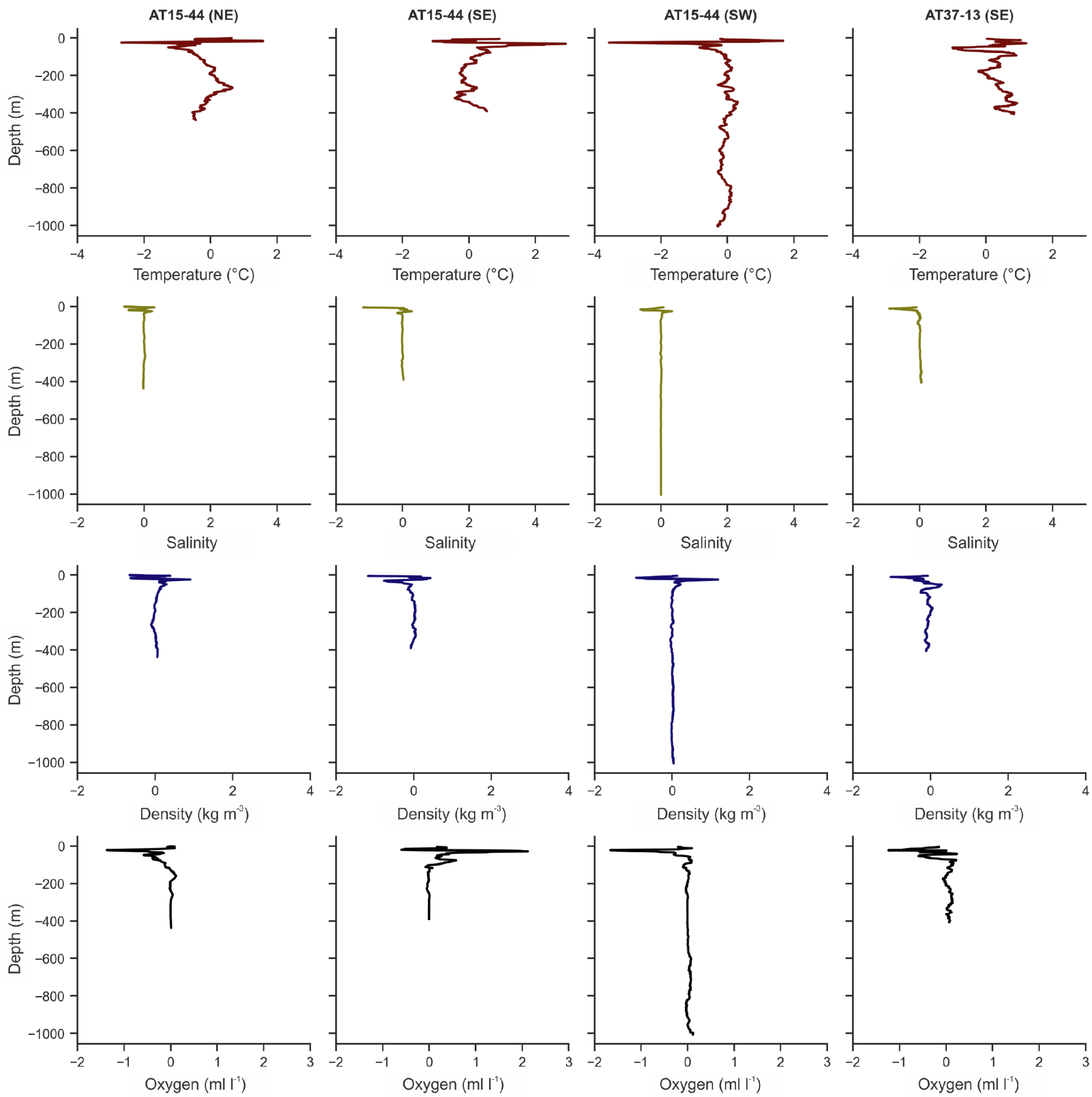

Figure 4. Spatial anomalies of temperature, salinity, density, and oxygen, at stations NE, SE, and SW, with respect to the averages of the Central station, from data measured by the RV 'Atlantis' CTD profiler during the AT15-44 campaign, and at station SE, with respect to the averages of the Central station, from data measured by the RV 'Atlantis' CTD profiler during the AT37-13 campaign.

'Atlantis' (Figure 6). Vertical extensions observed for water masses depended on the depth at which the CTD began or ended the sampling, so the full extension was not always recorded. The TSW was recorded during the AT15-59 campaign at depths extending from the surface to 58 m, corresponding to the maximum extension. The SSW showed subsurface salinity maximum between 19 m and

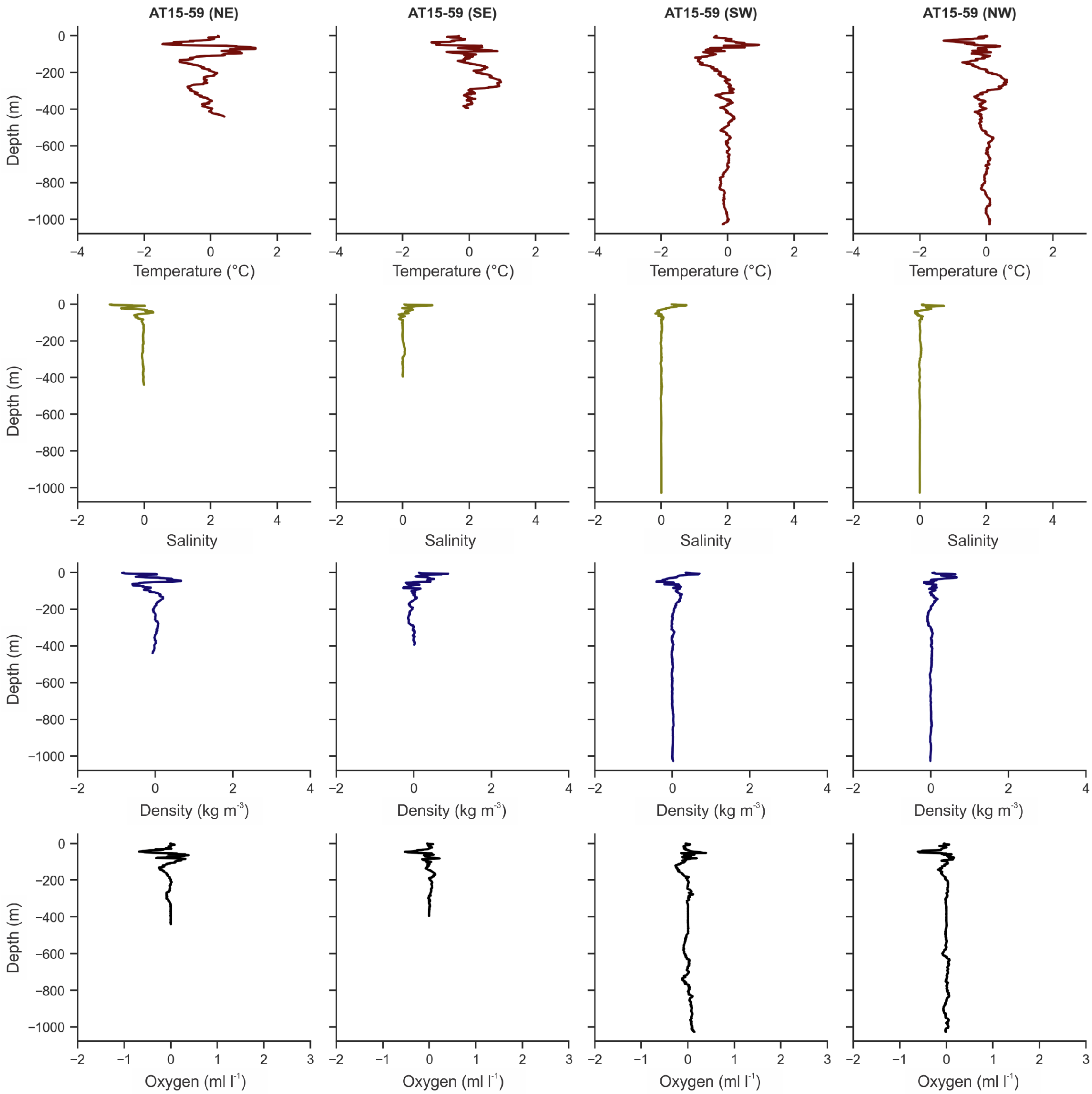

Figure 5. Spatial anomalies of temperature, salinity, density, and oxygen, at stations NE, SE, SW, and NW, with respect to the averages of the Central station, from data measured by the RV 'Atlantis' CTD profiler during the AT15-59 campaign.

344 m, with a maximum vertical extension of 210 m in the AT37-13 campaign. The AAIW was observed between 866 m and 1,061 m, with a maximum vertical extension of 161 m in the AT15-59 campaign (Table 3).

In general, profiles of the RV 'Atlantis' campaigns (Figures A2-A18) showed a decrease in dissolved oxygen until it reaches its minimum values in the core of the OMZ, while at greater depths it returns to higher values. Oxygen concentrations

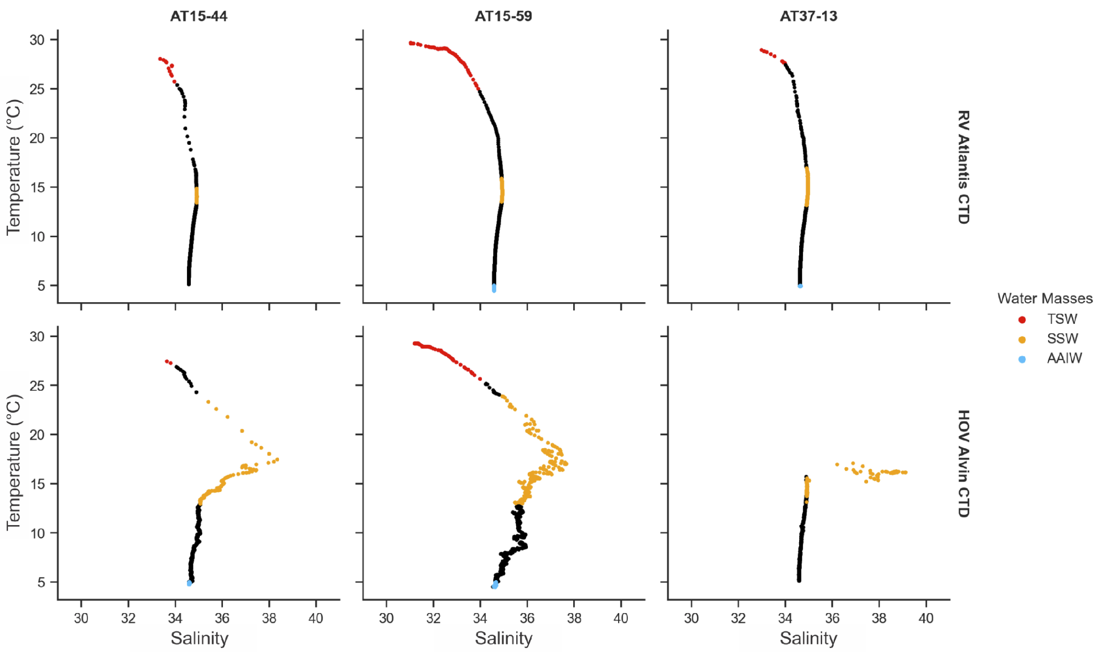

Figure 6. T-S diagrams of the averages at the Central station, from data measured by the RV 'Atlantis' CTD and HOV 'Alvin' CTD profilers during the AT15-44, AT15-59, and AT37-13 campaigns. Water masses are identified in red for Tropical Surface Water (TSW), orange for Subtropical Subsurface Water (SSW), and light blue for Antarctic Intermediate Water (AAIW).

Table 3. Depth of the upper and lower boundaries of the water masses in the averages at the Central station, from data measured by the RV 'Atlantis' CTD and HOV 'Alvin' CTD profilers during the AT15-44, AT15-59, and AT37-13 campaigns. TSW stands for Tropical Surface Water, SSW for Subtropical Subsurface Water, AAIW for Antarctic Intermediate Water, and VE for vertical extension.

		TSW			SSW			AAIW		
		Upper (m)	Lower (m)	VE (m)	Upper (m)	Lower (m)	VE (m)	Upper (m)	Lower (m)	VE (m)
'Atlantis'	AT15-44	0	13	13	65	131	66			
	AT15-59	0	55	55	129	207	78	866	1,027	161
	AT37-13	4	14	14	79	289	210	990	1,000	10
'Alvin'	AT15-44	1	3	3	19	160	141	1,007	1,061	54
	AT15-59	1	58	58	70	268	198	897	1,027	130
	AT37-13				156	344	188			

are highly variable above the OMZ, more stable within it, and slightly variable below it (for example, ranges in Appendix figures were described by horizontal dashed lines to represent the upper and lower boundaries of the OMZ). Oxygen profiles of samplings in the vicinity of the hydrothermal vents and in other stations in the ETP, from data measured by the RV 'Atlantis' CTD, were dominated by the presence of the OMZ. The upper edge of the OMZ in the 33 samplings with the RV 'Atlantis' CTD, for the three campaigns, was located within a range of depths from 35 m to 241 m. For the 24 samplings including the full extension of the OMZ, the lower edge ranged between 758 m and 1,117 m and the vertical extension of the OMZ ranges between 580 m and 1,082 m (Table A5). The minimum of oxygen observed in the core of the OMZ ranged from 0.0177 ml l^{-1} to 0.1034 ml l^{-1}, and was located between 320 m and 521 m deep (Table A1).

Regarding the seven casts of the FK190106 campaign (Figures 7 and 8), a remarkable OMZ can be observed in the oxygen profiles, which follow

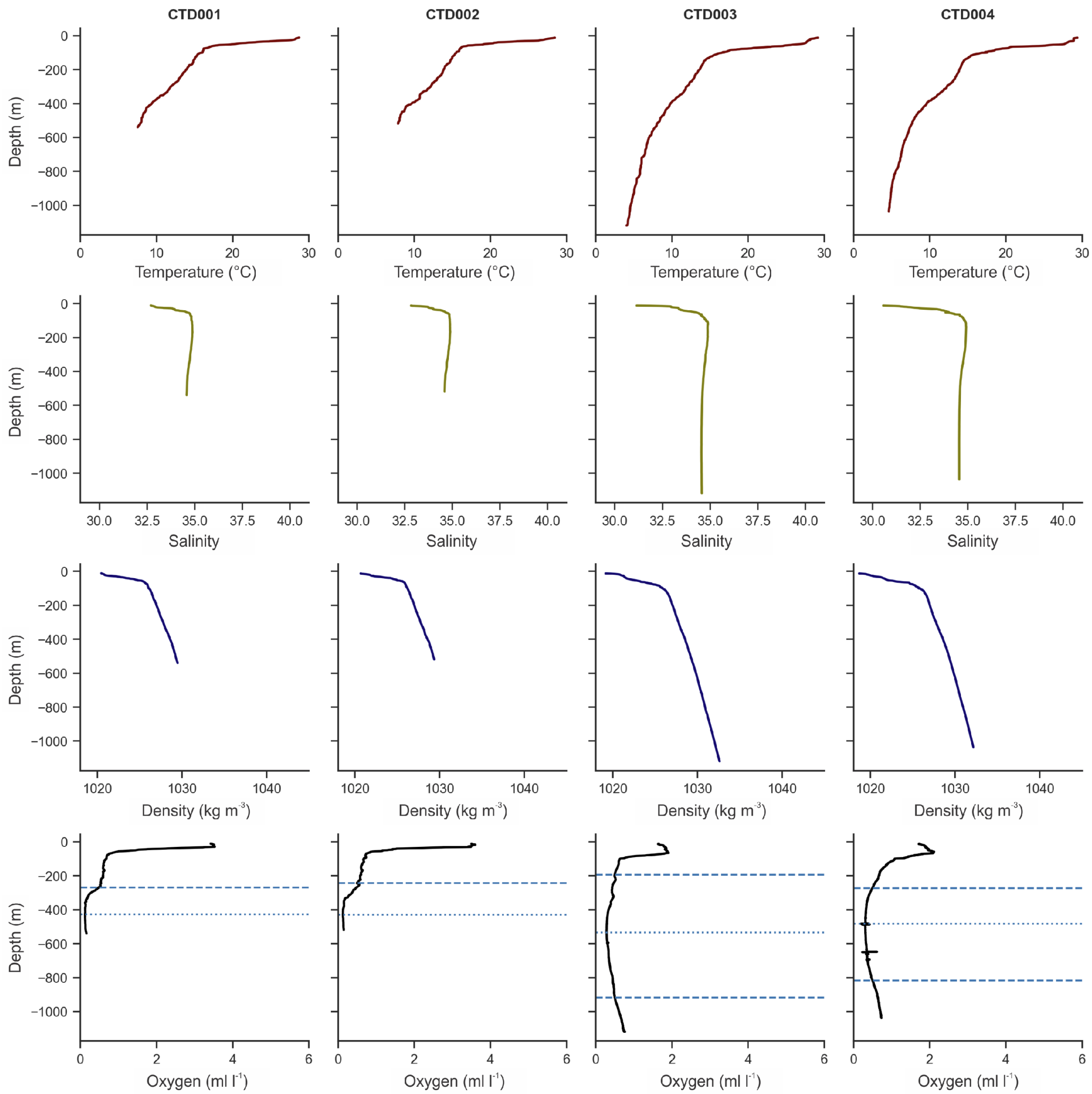

Figure 7. Temperature, salinity, density, and oxygen, at stations 1, 2, 3, and 4, from data measured by the RV 'Falkor' CTD profiler during the FK190106 campaign. In the oxygen profiles, the horizontal dashed lines represent the upper and lower boundaries of the OMZ (dissolved oxygen < 0.5 ml l^{-1}), and the horizontal dotted lines indicate the minimum oxygen.

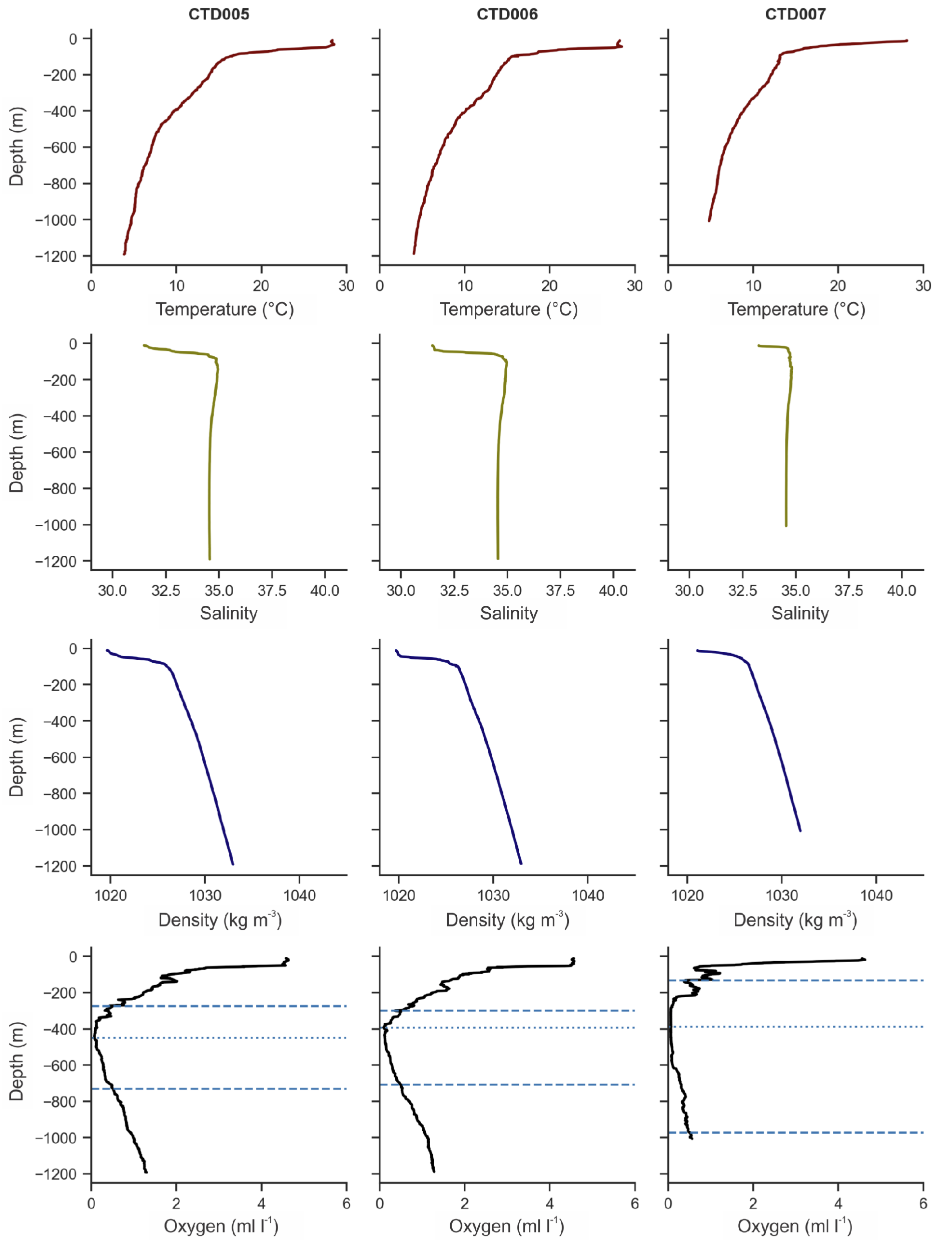

Figure 8. Temperature, salinity, density, and oxygen, at stations 5, 6, and 7, from data measured by the RV 'Falkor' CTD profiler during the FK190106 campaign. In the oxygen profiles, the horizontal dashed lines represent the upper and lower boundaries of the OMZ (dissolved oxygen < 0.5 ml l^{-1}), and the horizontal dotted lines indicate the minimum oxygen.

the same trends seen in the case of the RV 'Atlantis' campaigns. The OMZ was defined by an upper edge within a range from 132 m to 298 m, a lower edge from 708 m to 971 m, and a full extension between 410 m and 839 m (Table 4). The oxygen minimum observed in the core of the OMZ ranged from 0.0599 ml l^{-1} to 0.2797 ml l^{-1}, and was bounded by depths between 387 m and 534 m (Table A3).

Table 4. Oxygen concentration and depth of the upper and lower boundaries, and vertical extension, of the OMZ, for every station, from data measured by the RV 'Falkor' CTD profiler during the FK190106 campaign.

	Upper (ml l^{-1})	Depth (m)	Lower (ml l^{-1})	Depth (m)	Vertical extension (m)
CTD001	0.4876	267			
CTD002	0.4975	243			
CTD003	0.4976	192	0.4986	917	725
CTD004	0.4964	272	0.4990	817	545
CTD005	0.4259	273	0.4996	729	456
CTD006	0.4992	298	0.4992	708	410
CTD007	0.3987	132	0.4953	971	839

Oxygen profiles of the seven casts studied from the JC112 campaign (Figures 9 and 10) presented the same trends as the profiles obtained from other campaigns, with a OMZ extending from an upper edge located between 127 m and 206 m, and a lower edge from 719 m to 897 m, with a thickness between 520 m and 721 m (Table 5). The oxygen minimum observed in the core of the OMZ ranged from 0.0155 ml l^{-1} to 0.0202 ml l^{-1} and was located between 343 m and 466 m (Table A4).

In profiles reaching depths greater than 2,000 m, oxygen concentrations tended to stabilize with increasing depth (Tables 6-8).

With respect to temperature, salinity, and density, obtained profiles from data sampled during the five campaigns in the study area (Figures A2-A18) followed the characteristics described above for the profiles of the averages at the Central station (Figure 2; Tables A4, A7-A9). In particular, profiles from data measured by the RV 'Atlantis' CTD were delimited by a temperature within a range from 2.05 °C observed at 2,227 m depth to 29.98 °C at 5 m, a salinity from 29.99 at 2 m to 35.02 at 143 m, and a density from 1,018.01 kg m^{-3} at 2 m to 1,038.04 kg m^{-3} at 2,227 m (Tables 9 and 10). Profiles from data sampled by the HOV 'Alvin' CTD covered temperatures from 2.07 °C at 2,228 m to 29.79 °C at 2 m, salinities from 30.82 at 3 m to 40.71 at 27 m, and densities from 1,018.84 kg m^{-3} at 2 m to 1,038.05 kg m^{-3} at 2,225 m (Tables 9 and 10).

In the case of the RV 'Falkor' campaign, ranges for the profiles of variables corresponded to temperatures from 3.84 °C at 1,192 m to 29.38 °C at 12 m, salinity from 30.56 at 12 m to 34.98 at 105 m, and density from 1,018.66 kg m^{-3} at 12 m to 1,032.99 kg m^{-3} at 1,192 m (Figures 7 and 8; Tables 11 and 12).

As with the RRS 'James Cook' campaign, ranges for the samplings were defined by a temperature from 1.81 °C at 2633 m to 29.46 °C at 6 m, a salinity from 29.06 at 8 m to 34.96 at 140 m, and a density from 1,017.69 kg m^{-3} at 3 m to 1,042.77 kg m^{-3} at 3,272 m (Tables 13 and 14).

DISCUSSION

Our analysis has not only revealed the existence of TSW, SSW and AAIW in the study region but also allowed the characterization of the OMZ, since it was observed that within the boundaries of an OMZ oxygen continuously decreases with depth, stabilizes at the lowest concentration in the core or microxic zone and then increases slightly to the seafloor (Levin 2002). Along with this, results also showed spatial and time variability. Disturbances in the currents and upwelling systems mentioned above that supply oxygen to the ETP could be related to the temporal and spatial var-

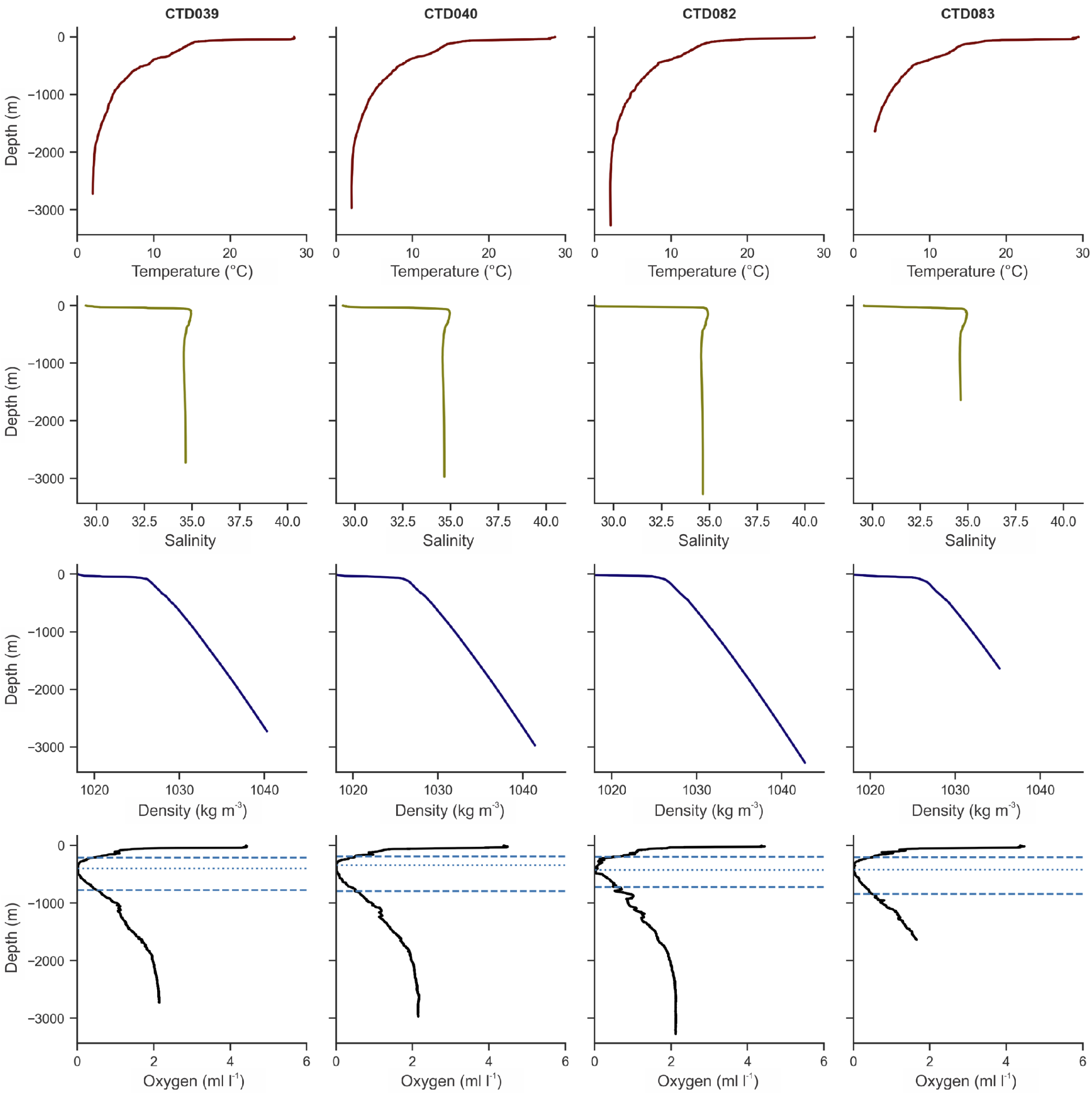

Figure 9. Temperature, salinity, density, and oxygen, at stations 39, 40, 82, and 83, from data measured by the RV 'James Cook' CTD profiler during the JC112 campaign. In the oxygen profiles, the horizontal dashed lines represent the upper and lower boundaries of the OMZ (dissolved oxygen < 0.5 ml l^{-1}), and the horizontal dotted lines indicate the minimum oxygen.

iability of the OMZs (Stramma et al. 2010). The arrival of TSW at the ETP for example, causes stratification, in turn modifying the depth of the oxycline, as happened during El Niño 2015-2016 when oxygen-rich tropical water accessed deeper layers (Trucco-Pignata et al. 2019). Furthermore, higher stratification and warmer temperatures decrease biological productivity reducing the supply

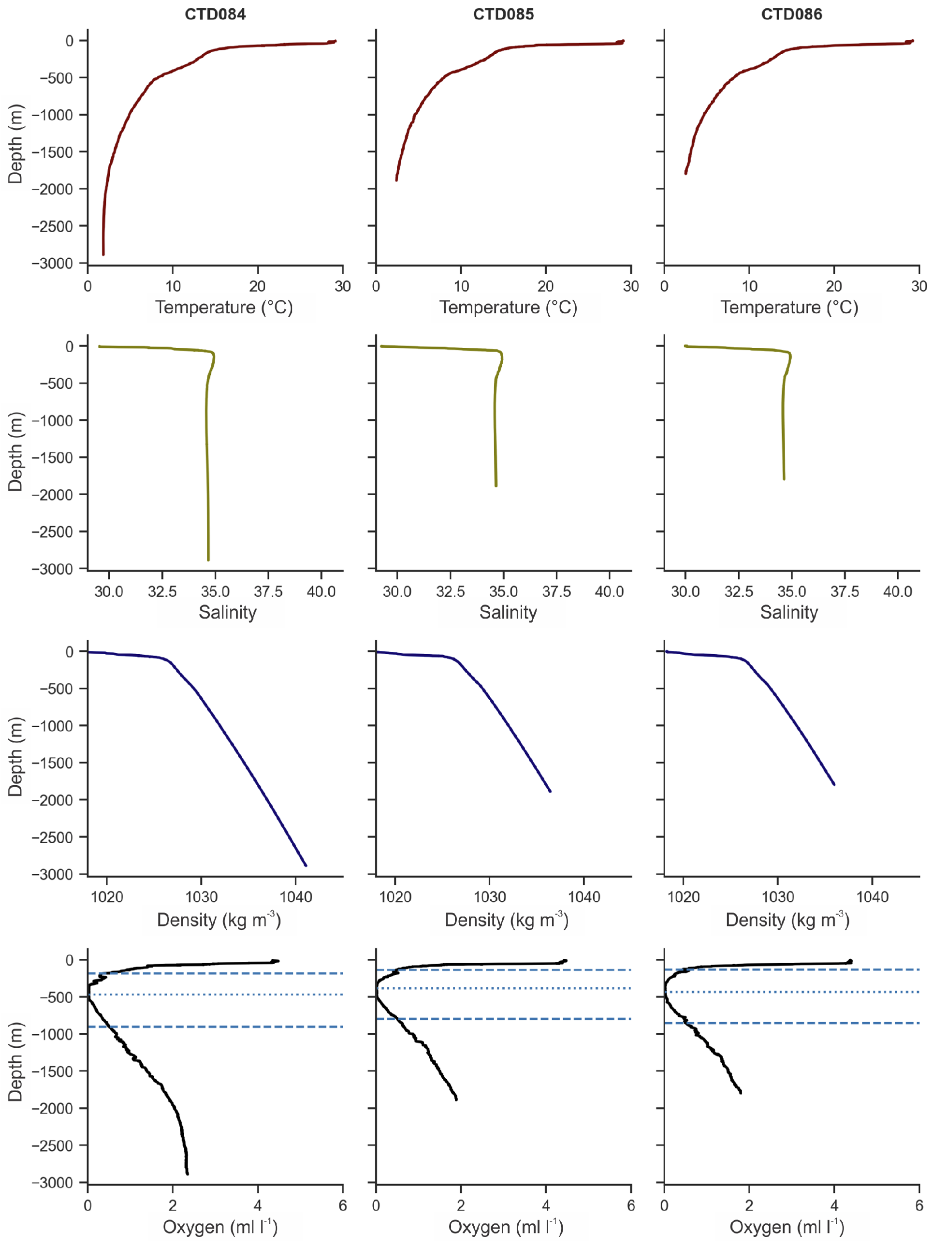

Figure 10. Temperature, salinity, density, and oxygen, at stations 84, 85, and 86, from data measured by the RV 'James Cook' CTD profiler during the JC112 campaign. In the oxygen profiles, the horizontal dashed lines represent the upper and lower boundaries of the OMZ (dissolved oxygen < 0.5 ml l^{-1}), and the horizontal dotted lines indicate the minimum oxygen.

of nutrients and the oxygen consumption, leading to a deeper, warmer, and more oxygen-rich thermocline as suggested by the correlation between heat content, respiration rates, and ENSO (Ito and Deutsch 2013; Trucco-Pignata et al. 2019). Nevertheless, Ito et al. (2019) affirm that during a positive PDO event the oxygen concentrations are high in the ETP, based on models and observations.

Table 5. Oxygen concentration and depth of the upper and lower boundaries, and vertical extension, of the OMZ, for every station, from data measured by the RV 'James Cook' CTD profiler during the JC112 campaign.

	Upper (ml l^{-1})	Depth (m)	Lower (ml l^{-1})	Depth (m)	Vertical extension (m)
CTD039	0.4785	206	0.4907	769	563
CTD040	0.4997	192	0.4964	793	601
CTD082	0.4836	199	0.4993	719	520
CTD083	0.4879	205	0.4970	844	639
CTD084	0.4863	179	0.4999	897	718
CTD085	0.4988	133	0.4981	793	660
CTD086	0.4369	127	0.4940	848	721

Table 6. Descriptive statistics of oxygen concentration and depth of the upper and lower boundaries, and vertical extension, of the OMZ, and of maximum and minimum values of oxygen with their respective depth, for every station, from data measured by the RV 'Atlantis' CTD profiler during the AT15-44, AT15-59, and AT37-13 campaigns.

	Upper (ml l^{-1})	Depth (m)	Lower (ml l^{-1})	Depth (m)	Vertical extension (m)	Minimum (ml l^{-1})	Depth (m)	Maximum (ml l^{-1})	Depth (m)
Count	33	33	24	24	24	33	33	33	33
Mean	0.4780	125.88	0.4960	892.04	762.67	0.0445	392.64	4.5143	12.15
Std	0.0264	61.25	0.0047	105.24	140.37	0.0175	58.86	0.2935	5.04
Min.	0.3742	35	0.4777	758	580	0.0177	320	3.7009	5
25%	0.4751	65	0.4945	782.5	639	0.0388	347	4.3204	8
50%	0.4850	142	0.4977	914	751	0.0401	371	4.6064	11
75%	0.4945	167	0.4986	959	838.75	0.0576	436	4.6559	16
Max.	0.4994	241	0.5000	1117	1,082	0.1034	521	5.2268	26

The strength of a PDO event is associated with the depth of the thermocline, whose influence on biological productivity and the changes in circulation due to PDO events affect oxygen concentrations (Deutsch et al. 2011; Duteil et al. 2018).

In the long term, observations in the Eastern Tropical North Pacific (ETNP) evidence that the vertical extent of the OMZ has increased, at both the upper and lower edges, and oxygen depletion is more severe (Fee 2012). The uncertainties of the global climate models are originated by the lack of a detailed study of the influence of global physical changes over biogeochemical processes and ecosystems and the wrong representation of submesoscale and mesoscale features due to a coarse resolution (Rixen et al. 2020).

The influence of climate change on open ocean OMZs is uncertain, due to inconsistencies between predictions of different models and measurements. It is possible that a warmer ocean under a nutrient enrichment fosters the extension and strengthening of OMZs, in accordance with the results of climate and biogeochemical models (Levin 2002; Matear and Hirst 2003; Oschlies et al. 2008; Breitburg et al. 2018). However, numerical models of the tropical oceans showed increased deoxygenation

Table 7. Descriptive statistics of oxygen concentration and depth of the upper and lower boundaries, and vertical extension, of the OMZ, and of maximum and minimum values of oxygen with their respective depth, for every station, from data measured by the RV 'Falkor' CTD profiler during the FK190106 campaign, with their respective depth.

	Upper (ml l^{-1})	Depth (m)	Lower (ml l^{-1})	Depth (m)	Vertical extension (m)	Minimum (ml l^{-1})	Depth (m)	Maximum (ml l^{-1})	Depth (m)
Count	7	7	5	5	5	7	7	7	7
Mean	0.4718	239.57	0.4983	828.40	595	0.1331	442.86	3.5710	34
Std	0.0416	58.00	0.0017	114.77	181.99	0.0786	51.93	1.1632	19.35
Min.	0.3987	132	0.4953	708	410	0.0599	387	1.9130	17
25%	0.4568	217.5	0.4986	729	456	0.0764	409	2.8231	21
50%	0.4964	267	0.4990	817	545	0.1222	428	3.6038	27
75%	0.4976	272.5	0.4992	917	725	0.1587	466.5	4.5996	43.5
Max.	0.4992	298	0.4996	971	839	0.2797	534	4.6348	65

Table 8. Descriptive statistics of oxygen concentration and depth of the upper and lower boundaries, and vertical extension, of the OMZ, and of maximum and minimum values of oxygen with their respective depth, for every station, from data measured by the RV 'James Cook' CTD profiler during the JC112 campaign, with their respective depth.

	Upper (ml l^{-1})	Depth (m)	Lower (ml l^{-1})	Depth (m)	Vertical extension (m)	Minimum (ml l^{-1})	Depth (m)	Maximum (ml l^{-1})	Depth (m)
Count	7	7	7	7	7	7	7	7	7
Mean	0.4817	177.29	0.4965	809.00	631.71	0.0176	408.57	4.4599	16.86
Std	0.0212	33.60	0.0032	58.74	75.74	0.0014	39.23	0.0303	5.15
Min.	0.4369	127	0.4907	719	520	0.0155	343	4.4068	11
25%	0.4810	156	0.4952	781	582	0.0170	390	4.4441	13.5
50%	0.4863	192	0.4970	793	639	0.0174	420	4.4743	17
75%	0.4933	202	0.4987	846	689	0.0180	425.5	4.4784	18.5
Max.	0.4997	206	0.4999	897	721	0.0202	466	4.4930	26

in the Pacific and Atlantic, while according to observations in the ETP oxygen has been persistently declining and OMZs have expanded over the last few decades and in the Indian Ocean oxygen has been stable for the last 30 years (Stramma et al. 2008; Stramma et al. 2010; Czeschel et al. 2012; Breitburg et al. 2018).

Ocean warming can reduce water solubility and weaken vertical mixing, decreasing oxygen supply to intermediate waters and intensifying deoxygenation in OMZs (Matear and Hirst 2003; Breitburg et al. 2018; Rixen et al. 2020; Sarma et al. 2020). In addition, deoxygenation favors the production of trace gasses associated with climate change, which could be released to the atmosphere by nearby coastal upwelling systems triggering feedback on global warming (Stramma et al. 2012; Loescher et al. 2016). Increased biological production due to eutrophication could lead to the accumulation of organic matter, such as zooplankton carcasses,

Table 9. Maximum and minimum values of temperature and salinity, for all the stations, from data measured by the RV 'Atlantis' CTD and HOV 'Alvin' CTD profilers during the AT15-44, AT15-59, and AT37-13 campaigns, with their respective depth and station ID.

		Temperature (°C)	Depth (m)	ID	Salinity	Depth (m)	ID
'Atlantis'	Max.	29.98	5	AT15-59-1	35.02	143	AT37-13-3
	Min.	2.05	2,227	AT15-44-12	29.99	2	AT15-59-2
'Alvin'	Max.	29.79	2	AT37-13-4909	40.71	27	AT15-44-4501
	Min.	2.07	2,228	AT15-44-4507	30.82	3	AT15-59-4587

Table 10. Maximum and minimum values of density and oxygen, for all the stations, from data measured by the RV 'Atlantis' CTD and HOV 'Alvin' CTD profilers during the AT15-44, AT15-59, and AT37-13 campaigns, with their respective depth and station ID.

		Density (kg m^{-3})	Depth (m)	ID	Oxygen (ml l^{-1})	Depth (m)	ID
'Atlantis'	Max.	1,038.04	2,227	AT15-44-12	5.2268	15	AT37-13-1
	Min.	1,018.01	2	AT15-59-2	0.0177	444	AT37-13-1
'Alvin'	Max.	1,038.05	2,225	AT15-44-4507			
	Min.	1,018.84	2	AT15-59-4587			

Table 11. Maximum and minimum values of temperature and salinity, for all the stations, from data measured by the RV 'Falkor' CTD profiler during the FK190106 campaign, with their respective depth and station ID.

	Temperature (°C)	Depth (m)	ID	Salinity	Depth (m)	ID
Max.	29.38	12	CTD004	34.98	105	CTD006
Min.	3.84	1,192	CTD005	30.56	12	CTD004

Table 12. Maximum and minimum values of density and oxygen, for all the stations, from data measured by the RV 'Falkor' CTD profiler during the FK190106 campaign, with their respective depth and station ID.

	Density (kg m^{-3})	Depth (m)	ID	Oxygen (ml l^{-1})	Depth (m)	ID
Max.	1,032.99	1,192	CTD005	4.6348	23	CTD005
Min.	1,018.66	12	CTD004	0.0599	387	CTD007

Table 13. Maximum and minimum values of temperature and salinity, for all the stations, from data measured by the RV 'James Cook' CTD profiler during the JC112 campaign, with their respective depth and station ID.

	Temperature (°C)	Depth (m)	ID	Salinity	Depth (m)	ID
Max.	29.46	6	CTD083	34.96	140	CTD039
Min.	1.81	2,633	CTD084	29.06	8	CTD082

Table 14. Maximum and minimum values of density and oxygen, for all the stations, from data measured by the RV 'James Cook' CTD profiler during the JC112 campaign, with their respective depth and station ID.

	Density (kg m^{-3})	Depth (m)	ID	Oxygen (ml l^{-1})	Depth (m)	ID
Max.	1,042.77	3,272	CTD082	4.4930	26	CTD040
Min.	1,017.69	3	CTD082	0.0155	380	CTD085

resulting in further deoxygenation and loss of nitrogen through denitrification and anammox processes (Levin 2002; DeVries et al. 2013; Glud et al. 2015; Stief et al. 2017; Rixen et al. 2020; Sarma et al. 2020). Conversely, a decrease in the export of organic matter could counteract the loss of oxygen caused by lower solubility and decreased vertical mixing (Sarma et al. 2020). Works mentioned in this paragraph suggest that a thickening of the OMZ could be expected in the future. Therefore, long term monitoring or research based on numerical models are future lines of research, since existing *in situ* measurements are insufficient to allow a time series approach, in particular, in a region with important natural climate variability.

The analysis of *in situ* CTD observations also enables additional future research. For example, the estimation of other derived variables like geostrophic currents (Brenes et al. 2016) and for the comparison of physical model outputs with numerical models results (Mora-Escalante et al. 2020). Additionally, Sarma et al. (2020) mentioned that results of numerical models could be improved considering biological variables like phytoplankton composition and including processes such as the transport of organic matter from the continental shelf and sinking carbon fluxes. Further studies of source waters, transport timescales, and export production are necessary to better understand the processes controlling oxygen levels within an OMZ and to improve the modeling of its evolution (Fu et al. 2018; Rixen et al. 2020). Also, more measurements are needed to fully understand the responses of the nitrogen cycle and other vital processes to low oxygen levels, especially under anoxic conditions (Rixen et al. 2020).

ACKNOWLEDGMENTS

This project was supported by several Vicerrectoría de Investigación, Universidad de Costa Rica projects: B5298, C2103, A5037, B9454, B0810, A1715, C0610, C1403, C0074, B7286, A4906 and A5719. Authors thank to the UCR School of Physics for giving us the research time to develop this study and to the UCR research centers CIMAR and CIGEFI for their logistic support during the data compilation and analysis. We are grateful to Lisa

Levin and Eric Cordes, for considering us as UCR scientist participants during the campaigns. Finally, we also thank to all the crew members of the 'Atlantis', 'Alvin', 'Falkor' and 'James Cook' vessels, for their collaboration during the data collection.

Declaration of interest

The authors have nothing to declare.

Author contributions

Alejandro Rodríguez: methodology, software, validation, formal analysis, investigation, resources, data curation, writing-original draft, visualization. Eric J. Alfaro: conceptualization, methodology, formal analysis, investigation, data curation, writing-review and editing, supervision, project administration, funding acquisition. Jorge Cortés: conceptualization, investigation, data curation, writing-review and editing, project administration, funding acquisition.

REFERENCES

ALFARO E, LIZANO O. 2001. Algunas relaciones entre las zonas de surgencia del Pacífico Centroamericano y los Océanos Pacífico y Atlántico Tropical. Rev Biol Trop. 49 (2): 185-193. https://www.kerwa.ucr.ac.cr/handle/10669/76681.

AMADOR JA, RIVERA ER, DURÁN-QUESADA AM, MORA G, SÁENZ F, CALDERÓN B, MORA N. 2016a. The easternmost tropical Pacific. Part I: a climate review. Rev Biol Trop. 64 (1): 1-22. DOI: https://doi.org/10.15517/rbt.v64i1.23407

AMADOR JA, DURÁN-QUESADA AM, RIVERA ER, MORA G, SÁENZ F, CALDERÓN B, MORA N. 2016b. The easternmost tropical Pacific. Part II: seasonal and intraseasonal modes of atmospheric variability. Rev Biol Trop. 64 (1): 23-57. DOI: https://doi.org/10.15517/rbt.v64i1.23409

BREITBURG D, LEVIN LA, OSCHLIES A, GRÉGOIRE M, CHAVEZ FP, CONLEY DJ, GARÇON V, GILBERT D, GUTIÉRREZ D, ISENSEE K, et al. 2018. Declining oxygen in the global ocean and coastal waters. Science. 359 (6371): eaam7240. DOI: http://doi.org/10.1126/science.aam7240

BRENES CL, COEN JE. 1985. Correlación T-S de las masas de agua en la región del Domo Térmico de Costa Rica. Uniciencia. 2 (1): 41-50. https://www.revistas.una.ac.cr/index.php/uniciencia/article/view/5350.

BRENES CL, BALLESTERO D, BENAVIDES R, SALAZAR, JP, MURILLO, G. 2016. Variations in the geostrophic circulation pattern and thermohaline structure in the Southeast Central American Pacific. Rev Biol Trop. 64 (2): 121-134. DOI: https://doi.org/10.15517/rbt.v64i1.23421

CABRÉ A, MARINOV I, BERNARDELLO R, BIANCHI D. 2015. Oxygen minimum zones in the tropical Pacific across CMIP5 models: mean state differences and climate change trends. Biogeosciences. 12 (18): 5429-5454. DOI: https://doi.org/10.5194/bg-12-5429-2015

CZESCHEL R, STRAMMA L, JOHNSON, G C. 2012. Oxygen decreases and variability in the eastern equatorial Pacific. J Geophys Res C Oceans. 117: C11019. DOI: https://doi.org/10.1029/2012JC008043

DALE AW, SOMMER S, LOMNITZ U, MONTES I, TREUDE T, LIEBETRAU V, GIER J, HENSEN C, DENGLER M, STOLPOVSKY K, et al. 2015. Organic carbon production, mineralisation and preservation on the Peruvian margin. Biogeosciences. 12 (5): 1537-1559. DOI: https://doi.org/10.5194/bg-12-1537-2015

DEUTSCH C, BRIX H, ITO T, FRENZEL H, THOMPSON, L. 2011. Climate-forced variability of ocean hypoxia. Science. 333 (6040): 336-339. DOI: http://doi.org/10.1126/science.1202422

DEVRIES T, DEUTSCH C, RAFTER PA, PRIMEAU F. 2013. Marine denitrification rates determined from a global 3-D inverse model. Biogeosciences. 10: 2481-2496. DOI: http://doi.org/10.5194/bg-10-2481-2013

Durán-Quesada AM, Sorí R, Ordoñez P, Gimeno L. 2020. Climate perspectives in the intra-Americas Seas. Atmosphere-Basel. 11 (9): 959. DOI: https://doi.org/10.3390/atmos11090959

Duteil O, Oschlies A, Böning, CW. 2018. Pacific Decadal Oscillation and recent oxygen decline in the eastern tropical Pacific Ocean. Biogeosciences. 15 (23): 7111-7126. DOI: https://doi.org/10.5194/bg-15-7111-2018

Enfield DB. 1987. The intraseasonal oscillation in eastern Pacific Sea levels: How is it forced? J Phys Oceanogr. 17: 1860-1876. DOI: https://doi.org/10.1175/1520-0485(1987)017<1860:TIOIEP>2.0.CO;2

Escoto-Murillo A, Alfaro EJ. 2021. Análisis de eventos fríos y cálidos por medio de datos de buceo: un enfoque de ciencia ciudadana en el Golfo de Papagayo, Costa Rica. Rev Biol Trop. 69 (2): 94-104. DOI: https://doi.org/10.15517/rbt.v69iSuppl.2.48309

Espinoza-Morriberón D, Echevin V, Colas F, Tam J, Gutierrez D, Graco M, Ledesma J, Quispe-Ccalluari C. 2019. Oxygen variability during ENSO in the tropical South Eastern Pacific. Front Mar Sci. 5: 526. DOI: https://doi.org/10.3389/fmars.2018.00526

Fee EA. 2012. Extent of the oxygen minimum zone in the Eastern Tropical North Pacific [thesis]. Proceedings from the University of Washington. School of Oceanography, Academic Year 2011-2012. 8 p. http://hdl.handle.net/1773/20061.

Fiedler PC, Mendelssohn R, Palacios DM, Bograd SJ. 2013. Pycnocline variations in the eastern tropical and North Pacific, 1958-2008. J Climate. 26 (2): 583-599. DOI: https://doi.org/10.1175/JCLI-D-11-00728.1

Fiedler PC, Talley LD. 2006. Hydrography of the eastern tropical Pacific: a review. Prog Oceanog. 69 (2-4): 143-180. DOI: https://doi.org/10.1016/j.pocean.2006.03.008

Fu W, Bardin A, Primeau F. 2018. Tracing ventilation source of tropical Pacific oxygen minimum zones with an adjoint global ocean transport model. Deep-Sea Res Pt I. 139: 95-103. DOI: https://doi.org/10.1016/j.dsr.2018.07.017

Fuenzalida R, Schneider W, Garcés-Vargas J, Bravo L, Lange C. 2009. Vertical and horizontal extension of the oxygen minimum zone in the eastern South Pacific Ocean. Deep-Sea Res Pt II. 56 (16): 992-1003. DOI: https://doi.org/10.1016/j.dsr2.2008.11.001

García-Franco JL, Chadwick R, Gray LJ, Osprey S, Adams DK. 2023. Revisiting mechanisms of the Mesoamerican Midsummer drought. Clim Dyn. 60: 549-569. DOI: https://doi.org/10.1007/s00382-022-06338-6

Glud RN, Grossart HP, Larsen M, Tang KW, Arendt KE, Rysgaard S, Thamdrup B, Nielsen TG. 2015. Copepod carcasses as microbial hot spots for pelagic denitrification. Limnol Oceanog. 60 (6): 2026-2036. DOI: https://doi.org/10.1002/lno.10149

Gooday AJ, Bett BJ, Escobar E, Ingole B, Levin LA, Neira C, Raman AV, Sellanes, J. 2010. Habitat heterogeneity and its influence on benthic biodiversity in oxygen minimum zones. Mar Ecol. 31 (1): 125-147. DOI: http://doi.org/10.1111/j.1439-0485.2009.00348.x

Gruber N, Lachkar Z, Frenzel H, Marchesiello P, Münnich M, McWilliams JC, Nagai T, Plattner, GK. 2011. Eddy-induced reduction of biological production in eastern boundary upwelling systems. Nat Geosci. 4 (11): 787-792. DOI: https://doi.org/10.1038/ngeo1273

Helly JJ, Levin LA. 2004. Global distribution of naturally occurring marine hypoxia on continental margins. Deep-Sea Res Pt I. 51 (9): 1159-1168. DOI: https://doi.org/10.1016/j.dsr.2004.03.009

Ito T, Deutsch C. 2013. Variability of the oxygen minimum zone in the tropical North Pacific during the late twentieth century. Global Biogeochem Cycles. 27 (4): 1119-1128. DOI: https://doi.org/10.1002/2013GB004567

Ito T, Long MC, Deutsch C, Minobe S, Sun D. 2019. Mechanisms of low-frequency Oxygen variability in the North Pacific. Global Biogeochem Cycles. 33 (2): 110-124. DOI: https://doi.org/10.1029/2018GB005987

KARSTENSEN J, STRAMMA L, VISBECK M. 2008. Oxygen minimum zones in the eastern tropical Atlantic and Pacific oceans. Prog Oceanog. 77 (4): 331-350. DOI: https://doi.org/10.1016/j.pocean.2007.05.009

KIRCHMAN DL. 2021. Dead Zones: The loss of oxygen from rivers, lakes, seas, and the ocean. New York: Oxford University Press. 217 p.

LEVIN LA. 2002. Deep-ocean life where oxygen is scarce. Am Sci. 90 (5): 436-444. DOI: https://doi.org/10.1511/2002.33.436

LEVIN LA. 2003. Oxygen minimum zone benthos: adaptation and community response to hypoxia. In: GIBSON RN, ATKINSON RJA, editors. Oceanography and marine biology, an annual review. 41. London: CRC Press. p. 1-45.

LEVIN LA, ORPHAN VJ, ROUSE GW, RATHBURN AE, USSLER W, COOK GS, GOFFREDI SK, PEREZ EM, WAREN A, GRUPE BM, CHADWICK G, STRICKROTT B. 2012. A hydrothermal seep on the Costa Rica margin: middle ground in a continuum of reducing ecosystems. Proc R Soc B. 279: 2580-2588. DOI: http://doi.org/10.1098/rspb.2012.0205

LIZANO OG. 2016. Distribución espacio-temporal de la temperatura, salinidad y oxígeno disuelto alrededor del Domo Térmico de Costa Rica. Rev Biol Trop. 64 (1): 135-152. DOI: https://doi.org/10.15517/rbt.v64i1.23422

LOESCHER CR, BANGE HW, SCHMITZ RA, CALLBECK CM, ENGEL A, HAUSS H, KANZOW T, KIKO R, LAVIK G, LOGINOVA A, et al. 2016. Water column biogeochemistry of oxygen minimum zones in the eastern tropical North Atlantic and eastern tropical South Pacific oceans. Biogeosciences. 13 (12): 3585-3606. DOI: https://doi.org/10.5194/bg-13-3585-2016

MATEAR RJ, HIRST AC. 2003. Long-term changes in dissolved oxygen concentrations in the ocean caused by protracted global warming. Global Biogeochem Cycles. 17 (4): 1125. DOI: https://doi.org/10.1029/2002GB001997

MORA-ESCALANTE RE, LIZANO OG, ALFARO EJ, RODRÍGUEZ A. 2020. Distribución de temperatura y salinidad en campañas oceanográficas recientes en el Pacífico Tropical Oriental de Costa Rica. Rev Biol Trop. 68 (1): 177-197. DOI: https://doi.org/10.15517/rbt.v68iS1.41180

NEIRA C, INGELS J, MENDOZA G, HERNANDEZ-LOPEZ E, LEVIN LA. 2018. Distribution of meiofauna in bathyal sediments influenced by the Oxygen Minimum Zone off Costa Rica. Front Mar Sci. 5: 448. DOI: http://doi.org/10.3389/fmars.2018.00448

OSCHLIES A, SCHULZ KG, RIEBESELL U, SCHMITTNER A. 2008. Simulated 21st century's increase in oceanic suboxia by CO_2-enhanced biotic carbon export. Global Biogeochem Cycles. 22 (4): GB4008. DOI: https://doi.org/10.1029/2007GB003147

PAULMIER A, RUIZ-PINO D. 2009. Oxygen minimum zones (OMZS) in the modern ocean. Prog Oceanog. 80 (3-4): 113-128. DOI: http://doi.org/10.1016/j.pocean.2008.08.001

RIXEN T, COWIE G, GAYE B, GOES J, DO ROSÁRIO GOMES H, HOOD RR, LACHKAR Z, SCHMIDT H, SEGSCHNEIDER J, SINGH A. 2020. Reviews and syntheses: present, past, and future of the oxygen minimum zone in the northern Indian Ocean. Biogeosciences. 17 (23): 6051-6080. DOI: https://doi.org/10.5194/bg-17-6051-2020

RODRÍGUEZ A, ALFARO EJ, CORTÉS J. 2021. Spatial and temporal dynamics of the hydrology at Salinas Bay, Costa Rica, Eastern Tropical Pacific. Rev Biol Trop. 69 (2): 105-126. DOI: https://doi.org/10.15517/rbt.v69iSuppl.2.48314

ROSS-SALAZAR E, JIMÉNEZ-RAMÓN JA, CASTRO-CAMPOS M, BLANCO-BOLAÑOS M. 2019. Atlas Domo Térmico de Costa Rica. San José: Fundación MarViva. 108 p. https://marviva.net/atlas-del-domo-termico-de-costa-rica/.

SARMA VVSS, BHASKAR TU, KUMAR JP, CHAKRABORTY K. 2020. Potential mechanisms responsible for occurrence of core oxygen minimum zone in the north-eastern Arabian Sea. Deep-Sea Res Pt I. 165: 103393. DOI: https://doi.

org/10.1016/j.dsr.2020.103393
Sea-Bird Electronics. 2013. SBE 43 Dissolved oxygen sensor: application note no. 64. https://www.seabird.com.
Sea-Bird Electronics. 2016. Seasoft V2 SBE Data processing: software manual. https://www.seabird.com.
Stief P, Lundgaard ASB, Morales-Ramírez Á, Thamdrup B, Glud RN. 2017. Fixed-nitrogen loss associated with sinking zooplankton carcasses in a coastal oxygen minimum zone (Golfo Dulce, Costa Rica). Front Mar Sci. 4: 152. DOI: https://doi.org/10.3389/fmars.2017.00152
Stramma L, Johnson GC, Firing E, Schmidtko S. 2010. Eastern Pacific oxygen minimum zones: supply paths and multidecadal changes. J Geophys Res-Oceans. 115: C09011. DOI: https://doi.org/10.1029/2009JC005976
Stramma L, Johnson GC, Sprintall J, Mohrholz V. 2008. Expanding oxygen-minimum zones in the tropical oceans. Science. 320 (5876), 655-658. DOI: https://doi.org/10.1126/science.1153847
Stramma L, Oschlies A, Schmidtko S. 2012. Mismatch between observed and modeled trends in dissolved upper-ocean oxygen over the last 50 yr. Biogeosciences. 9 (10): 4045-4057. DOI: https://doi.org/10.5194/bg-9-4045-2012
Trucco-Pignata PN, Hernández-Ayón JM, Santamaria-del-Angel E, Beier E, Sánchez-Velasco L, Godínez VM, Norzagaray O. 2019. Ventilation of the upper oxygen minimum zone in the coastal region off Mexico: implications of El Niño 2015-2016. Front Mar Sci. 6: 459. DOI: https://doi.org/10.3389/fmars.2019.00459
Van Rossum G, Drake FL. 2009. Python 3 reference manual. Scotts Valley: CreateSpace. DOI: https://dl.acm.org/doi/book/10.5555/1593511
Wyrtki K. 1967. Circulation and water masses in the Eastern Equatorial Pacific Ocean. Int J Oceanol Limnol. 1 (2): 117-147. ftp://mananui.soest.hawaii.edu/pub/rlukas/Klaus/papers/Wyrtki1967%20IJOL.pdf.

APPENDIX

Table A1. Maximum and minimum values of oxygen with their respective depth, latitude, longitude, and date, for every station, from data measured by the RV 'Atlantis' CTD profiler during the AT15-44, AT15-59, and AT37-13 campaigns.

	Minimum (ml l^{-1})	Depth (m)	Maximum (ml l^{-1})	Depth (m) (m)	Latitude (°N)	Longitude (°W)	Date
AT15-44-1	0.0387	320	4.2001	11	8.93	84.32	02/21/2009
AT15-44-13	0.0401	371	4.6349	19	8.93	84.31	03/05/2009
AT15-44-2	0.0394	331	4.2215	11	9.02	84.20	02/22/2009
AT15-44-14	0.0393	369	4.6777	26	8.85	84.22	03/06/2009
AT15-44-5	0.0388	324	4.2607	14	8.87	84.43	02/25/2009
AT15-44-3	0.0396	347	4.3204	14	9.02	84.24	02/23/2009
AT15-44-4	0.0387	329	4.2890	8	8.98	84.27	02/24/2009
AT15-44-6	0.0389	323	4.3332	10	8.97	84.62	02/26/2009
AT15-44-7	0.0395	359	4.2336	14	9.09	84.58	02/27/2009
AT15-44-8	0.0401	377	4.2357	7	9.21	84.64	02/28/2009
AT15-44-9	0.0403	376	3.7009	5	10.30	86.31	03/02/2009
AT15-44-10	0.0399	350	3.9668	5	10.30	86.30	03/02/2009
AT15-44-11	0.0401	368	4.9680	8	9.22	84.93	03/03/2009
AT15-44-12	0.0395	354	4.4763	5	9.09	84.85	03/04/2009
AT15-59-1	0.0560	452	4.6615	16	8.93	84.31	01/06/2010
AT15-59-3	0.0558	430	4.6138	16	8.93	84.31	01/07/2010
AT15-59-5	0.0588	462	4.6648	11	8.92	84.30	01/08/2010
AT15-59-7	0.0576	463	4.6510	10	8.93	84.31	01/09/2010
AT15-59-8	0.0585	347	4.5873	7	8.92	84.30	01/10/2010
AT15-59-2	0.0591	344	4.6523	8	9.02	84.20	01/07/2010
AT15-59-4	0.0559	392	4.6165	9	8.85	84.22	01/08/2010
AT15-59-6	0.0600	357	4.6064	9	8.87	84.43	01/09/2010
AT15-59-9	0.0576	477	4.6216	6	9.02	84.41	01/10/2010
AT15-59-10	0.0560	334	4.6603	18	9.12	84.84	01/10/2010
AT15-59-11	0.0585	418	4.6559	16	9.12	84.84	01/11/2010
AT15-59-12	0.0601	345	4.5976	19	9.17	84.80	01/11/2010
AT37-13-1	0.0177	444	5.2268	15	8.93	84.31	05/22/2017
AT37-13-2	0.0205	436	5.0329	15	8.93	84.31	05/25/2017
AT37-13-5	0.1034	407	4.4701	13	8.85	84.22	06/03/2017
AT37-13-3	0.0195	492	4.6449	16	9.09	84.83	05/28/2017
AT37-13-4	0.0179	507	4.6636	14	9.12	84.84	05/29/2017
AT37-13-6	0.0219	431	4.4676	19	8.97	84.63	06/09/2017
AT37-13-7	0.0192	521	4.3566	7	8.80	85.18	06/09/2017

Table A2. Latitude, longitude, and date, for every station, from data measured by the HOV 'Alvin' CTD profiler during the AT15-44, AT15-59, and AT37-13 campaigns.

	Latitude (°N)	Longitude (°W)	Date
AT15-44-4501	8.93	84.31	02/22/2009
AT15-44-4502	8.93	84.31	02/23/2009
AT15-44-4503	8.93	84.31	02/24/2009
AT15-44-4504	8.92	84.30	02/25/2009
AT15-44-4505	8.92	84.30	02/26/2009
AT15-44-4511	8.93	84.31	03/05/2009
AT15-44-4506	8.96	84.64	02/27/2009
AT15-44-4507	8.94	84.64	02/28/2009
AT15-44-4508	9.03	84.62	03/01/2009
AT15-44-4509	9.12	84.84	03/03/2009
AT15-44-4510	9.17	84.80	03/04/2009
AT15-44-4512	9.02	84.50	03/06/2009
AT15-44-4513	9.12	84.84	03/07/2009
AT15-59-4586	8.93	84.31	01/07/2010
AT15-59-4587	8.93	84.31	01/08/2010
AT15-59-4588	8.93	84.31	01/09/2010
AT15-59-4589	8.93	84.31	01/10/2010
AT15-59-4590	9.12	84.84	01/11/2010
AT15-59-4591	9.12	84.84	01/12/2010
AT37-13-4909	8.93	84.31	05/24/2017
AT37-13-4911	9.12	84.84	05/26/2017
AT37-13-4912	9.12	84.84	05/27/2017
AT37-13-4913	9.12	84.84	05/28/2017
AT37-13-4914	9.12	84.84	05/29/2017
AT37-13-4915	9.12	84.84	05/30/2017

Table A3. Maximum and minimum values of oxygen, latitude, longitude, and date, for every station, from data measured by the RV 'Falkor' CTD profiler during the FK190106 campaign, with their respective depth.

	Minimum (ml l^{-1})	Depth (m)	Maximum (ml l^{-1})	Depth (m) (m)	Latitude (°N)	Longitude (°W)	Date
CTD001	0.1222	426	3.5304	29	8.87	84.24	01/10/2019
CTD002	0.1253	428	3.6038	17	8.84	84.23	01/11/2019
CTD003	0.2797	534	1.9130	65	8.05	85.77	01/16/2019
CTD004	0.1920	483	2.1157	58	6.91	85.88	01/17/2019
CTD005	0.0676	450	4.6348	23	5.42	87.20	01/20/2019
CTD006	0.0851	392	4.5714	27	5.04	87.44	01/21/2019
CTD007	0.0599	387	4.6278	19	9.70	85.92	01/26/2019

Table A4. Maximum and minimum values of oxygen, latitude, longitude, and date, for every station, from data measured by the RV 'James Cook' CTD profiler during the JC112 campaign, with their respective depth.

	Minimum (ml l^{-1})	Depth (m)	Maximum (ml l^{-1})	Depth (m) (m)	Latitude (°N)	Longitude (°W)	Date
CTD039	0.0174	400	4.4350	11	6.15	83.47	12/30/2014
CTD040	0.0168	343	4.4930	26	5.75	83.49	12/30/2014
CTD082	0.0202	421	4.4533	19	4.75	85.32	01/12/2015
CTD083	0.0178	420	4.4743	18	5.68	86.00	01/12/2015
CTD084	0.0172	466	4.4826	17	7.08	86.00	01/13/2015
CTD085	0.0155	380	4.4743	11	6.09	85.46	01/13/2015
CTD086	0.0182	430	4.4068	16	6.42	85.04	01/14/2015

Table A5. Oxygen concentration and depth of the upper and lower boundaries, and vertical extension, of the OMZ, for every station, from data measured by the RV 'Atlantis' CTD profiler during the AT15-44, AT15-59, and AT37-13 campaigns.

	Upper (ml l^{-1})	Depth (m)	Lower (ml l^{-1})	Depth (m)	Vertical extension (m)
AT15-44-1	0.4850	54	0.5000	956	902
AT15-44-13	0.4601	89	0.4993	915	826
AT15-44-2	0.4991	59			
AT15-44-14	0.4963	98			
AT15-44-5	0.4918	80	0.4976	913	833
AT15-44-3	0.3742	65			
AT15-44-4	0.4550	75			
AT15-44-6	0.4465	59	0.4973	915	856
AT15-44-7	0.4579	74	0.4983	891	817
AT15-44-8	0.4869	57			
AT15-44-9	0.4825	35	0.4948	1,117	1,082
AT15-44-10	0.4826	35	0.4945	1,099	1,064
AT15-44-11	0.4945	59	0.4978	972	913
AT15-44-12	0.4097	53	0.4933	926	873
AT15-59-1	0.4923	143	0.4980	787	644
AT15-59-3	0.4972	149	0.4978	816	667
AT15-59-5	0.4994	146	0.4988	786	640
AT15-59-7	0.4871	178	0.4987	758	580
AT15-59-8	0.4958	167	0.4937	772	605
AT15-59-2	0.4959	132			
AT15-59-4	0.4812	174			
AT15-59-6	0.4980	134	0.4997	770	636
AT15-59-9	0.4731	142	0.4999	772	630
AT15-59-10	0.4654	146	0.4944	771	625
AT15-59-11	0.4923	145	0.4986	769	624
AT15-59-12	0.4850	148			
AT37-13-1	0.4818	213	0.4963	893	680
AT37-13-2	0.4757	225	0.4929	915	690
AT37-13-5	0.4929	241			
AT37-13-3	0.4889	209	0.4985	980	771
AT37-13-4	0.4956	219	0.4902	950	731
AT37-13-6	0.4751	197	0.4777	998	801
AT37-13-7	0.4790	154	0.4962	968	814

Table A6. Maximum gradients of temperature, salinity, density, and oxygen, for every station, from data measured by the RV 'Atlantis' CTD profiler during the AT15-44, AT15-59, and AT37-13 campaigns, with their respective depth.

	Temperature (°C)	Depth (m)	Salinity	Depth (m)	Density (kg m^{-3})	Depth (m)	Oxygen (ml l^{-1})	Depth (m)
AT15-44-1	24.22	25	34.44	28	1,022.97	25	3.8133	23
AT15-44-13	28.51	8	32.84	5	1,021.05	8	4.4658	22
AT15-44-2	25.49	18	33.25	1	1,021.07	1	3.3123	20
AT15-44-14	28.81	6	32.31	6	1,020.13	6	4.3233	29
AT15-44-5	24.50	20	33.86	20	1,022.71	20	4.0721	18
AT15-44-3	23.86	23	34.00	23	1,023.02	23	3.4548	22
AT15-44-4	23.91	25	34.09	25	1,023.09	25	2.8257	27
AT15-44-6	24.46	19	33.53	12	1,022.76	19	4.0863	17
AT15-44-7	23.97	23	34.08	23	1,023.05	23	3.8574	21
AT15-44-8	25.92	10	33.75	10	1,022.16	10	4.2107	8
AT15-44-9	19.46	17	34.58	17	1,024.66	17	2.7891	15
AT15-44-10	20.29	18	34.52	18	1,024.40	18	3.2440	15
AT15-44-11	28.12	5	33.24	5	1,021.06	5	4.6128	5
AT15-44-12	26.82	7	34.02	7	1,022.07	7	3.7103	16
AT15-59-1	29.89	9	30.97	9	1,018.78	9	4.5429	8
AT15-59-3	29.43	15	31.31	15	1,019.22	15	3.9474	54
AT15-59-5	25.73	51	31.03	6	1,018.91	6	4.3099	46
AT15-59-7	26.20	54	31.67	9	1,019.48	9	4.0530	53
AT15-59-8	29.58	6	31.03	6	1,018.92	6	4.4903	5
AT15-59-2	29.81	7	30.13	5	1,018.13	5	4.5272	3
AT15-59-4	29.36	4	31.10	4	1,019.04	4	4.4887	2
AT15-59-6	27.27	51	31.48	4	1,019.34	4	4.2699	52
AT15-59-9	29.68	3	31.13	6	1,019.05	6	4.4670	4
AT15-59-10	25.18	51	32.49	17	1,020.25	17	4.1476	43
AT15-59-11	29.16	14	32.40	14	1,020.12	14	4.3909	33
AT15-59-12	29.18	15	32.36	15	1,020.09	15	4.4628	29
AT37-13-1	28.20	9	33.49	9	1,021.23	9	4.6119	25
AT37-13-2	26.48	21	33.28	9	1,020.85	9	4.6160	23
AT37-13-5	28.95	10	32.91	10	1,020.55	10	3.6600	25
AT37-13-3	27.97	15	33.27	12	1,020.79	12	3.8292	29
AT37-13-4	27.07	16	33.38	6	1,022.12	16	4.3508	24
AT37-13-6	27.88	25	32.72	9	1,021.64	25	4.1880	28
AT37-13-7	28.32	15	33.74	15	1,021.41	15	4.2930	14

Table A7. Maximum gradients of temperature, salinity, and density, for every station, from data measured by the HOV 'Alvin' CTD profiler during the AT15-44, AT15-59, and AT37-13 campaigns, with their respective depth.

	Temperature (°C)	Depth (m)	Salinity	Depth (m)	Density (kg m^{-3})	Depth (m)
AT15-44-4501	27.50	2	33.52	2	1,021.45	2
AT15-44-4502	23.53	20	40.25	29	1,026.42	25
AT15-44-4503	24.23	20	34.84	19	1,023.21	19
AT15-44-4504	22.37	21	36.22	21	1,025.13	21
AT15-44-4505	24.25	17	33.55	2	1,023.30	18
AT15-44-4511	27.14	2	33.95	2	1,021.89	2
AT15-44-4506	27.64	6	34.75	14	1,023.47	14
AT15-44-4507	27.44	6	33.58	6	1,021.53	6
AT15-44-4508	21.62	17	33.43	5	1,021.36	5
AT15-44-4509	27.68	3	33.86	3	1,021.66	3
AT15-44-4510	26.60	6	34.12	5	1,022.00	5
AT15-44-4512	28.14	9	32.74	9	1,020.69	9
AT15-44-4513	26.36	2	33.62	2	1,021.89	2
AT15-59-4586	28.95	18	32.09	7	1,020.27	18
AT15-59-4587	28.53	48	31.44	33	1,020.28	48
AT15-59-4588	27.24	61	33.47	61	1,021.75	61
AT15-59-4589	26.30	72	31.16	31	1,022.55	72
AT15-59-4590	24.74	68	35.79	82	1,024.99	82
AT15-59-4591	26.77	52	33.92	52	1,022.20	52
AT37-13-4909	29.79	2	33.34	9		
AT37-13-4911	28.46	15	32.45	4		
AT37-13-4912	27.53	14	32.62	1		
AT37-13-4913	27.53	21	32.89	10		
AT37-13-4914	26.00	27	33.00	3		

Table A8. Maximum gradients of temperature, salinity, density, and oxygen, for every station, from data measured by the RV 'Falkor' CTD profiler during the FK190106 campaign, with their respective depth.

	Temperature (°C)	Depth (m)	Salinity	Depth (m)	Density (kg m^{-3})	Depth (m)	Oxygen (ml l^{-1})	Depth (m)
CTD001	27.11	28	33.37	26	1021.60	27	3.2184	33
CTD002	26.33	29	32.90	14	1020.78	14	3.4887	30
CTD003	24.59	61	31.14	12	1019.16	12	1.6957	18
CTD004	22.89	63	30.56	12	1018.66	12	1.7320	14
CTD005	27.13	50	32.15	31	1021.39	49	4.3513	51
CTD006	26.20	53	32.00	44	1021.71	52	4.3495	53
CTD007	27.37	17	33.59	17	1021.61	17	4.4727	23

Table A9. Maximum gradients of temperature, salinity, density, and oxygen, for every station, from data measured by the RV 'James Cook' CTD profiler during the JC112 campaign, with their respective depth.

	Temperature (°C)	Depth (m)	Salinity	Depth (m)	Density (kg m^{-3})	Depth (m)	Oxygen (ml l^{-1})	Depth (m)
CTD039	26.35	46	30.47	30	1,021.69	46	4.1351	44
CTD040	28.06	35	31.30	34	1,019.78	34	3.7641	45
CTD082	24.86	27	29.18	15	1,017.84	15	3.9572	26
CTD083	28.65	39	29.67	10	1,017.96	9	2.4226	51
CTD084	27.72	43	30.43	17	1,018.60	16	4.3418	41
CTD085	26.78	49	29.49	9	1,017.96	9	3.5707	52
CTD086	29.04	12	30.55	15	1,018.48	12	4.1091	49

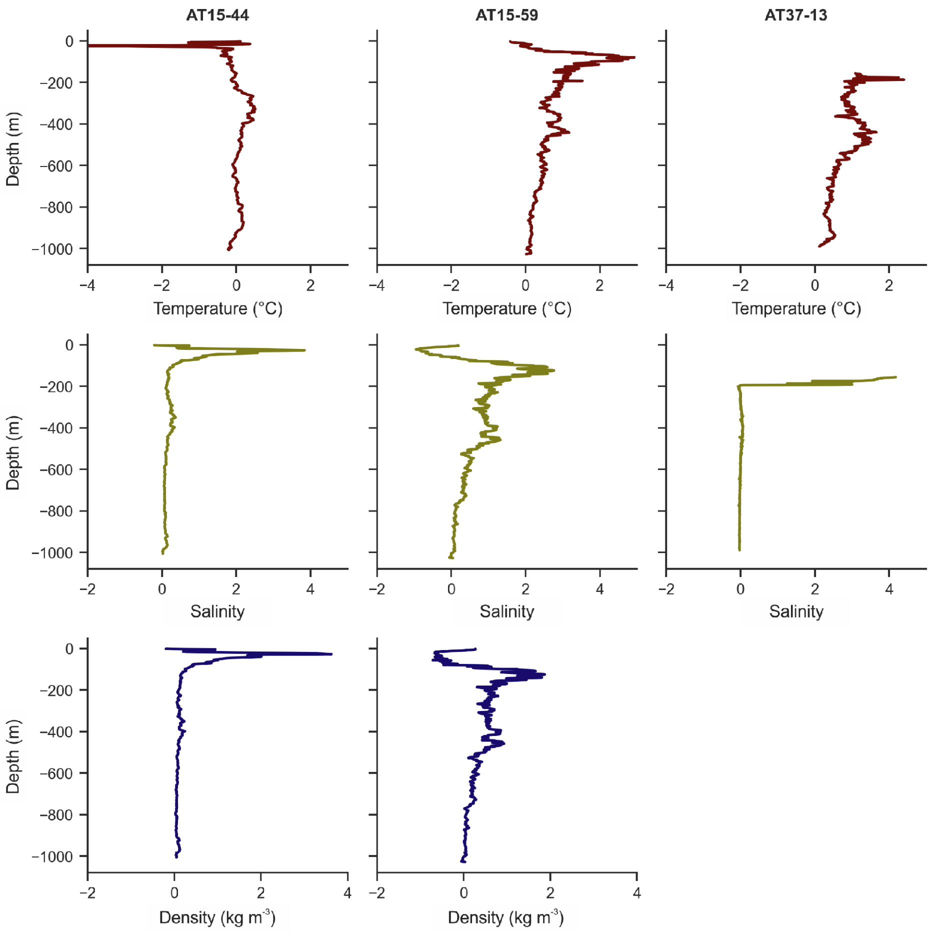

Figure A1. Anomalies of temperature, salinity, and density, for the averages of the Central station, from data measured by the HOV 'Alvin' CTD profiler, with respect to the averages of the Central station, from data measured by the RV 'Atlantis' CTD profiler, during the AT15-44, AT15-59, and AT37-13 campaigns.

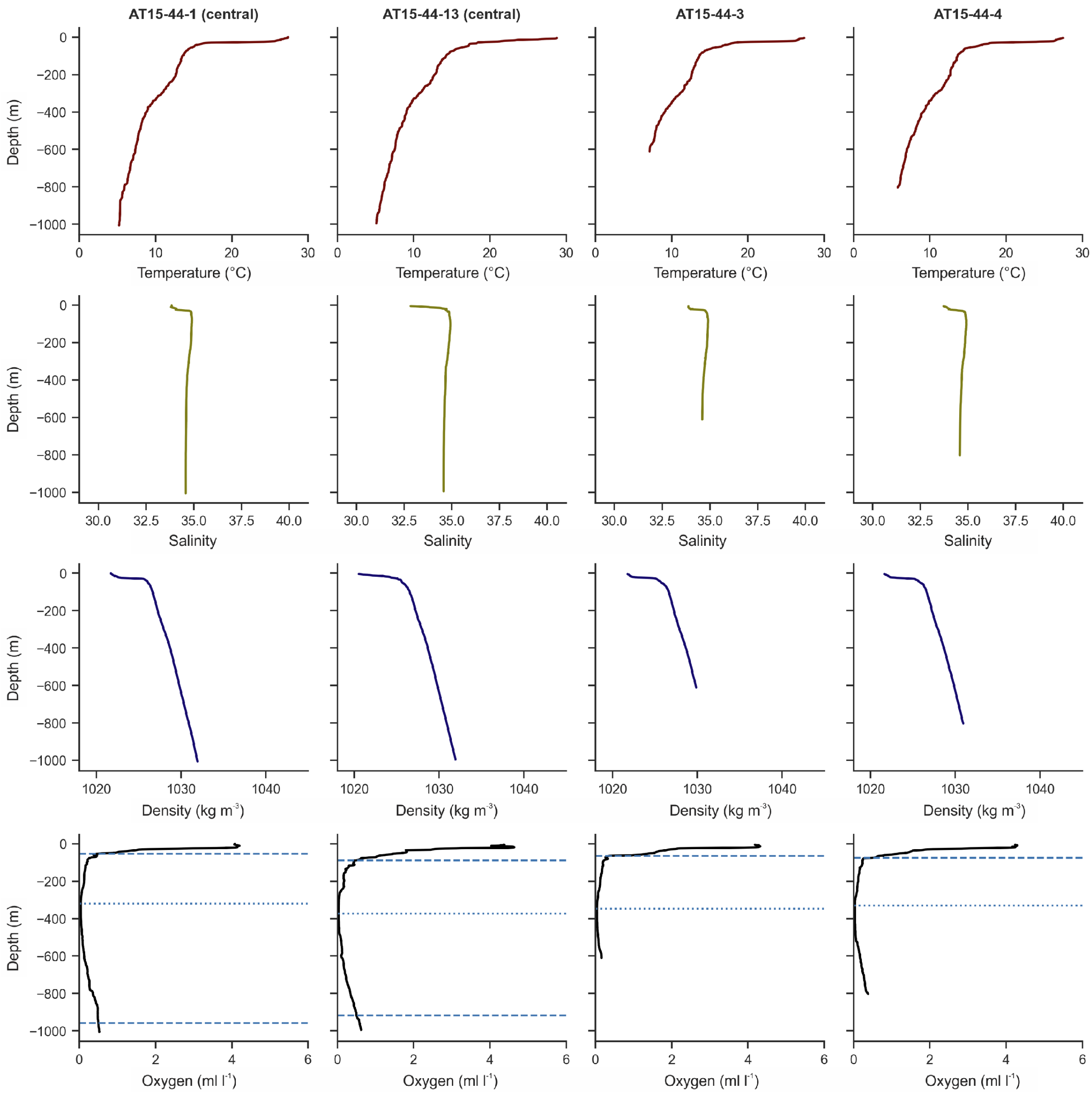

Figure A2. Temperature, salinity, density, and oxygen, at stations 1 and 13 (Central), and stations 3 and 4, from data measured by the RV 'Atlantis' CTD profiler during the AT15-44 campaign. In the oxygen profiles, the horizontal dashed lines represent the upper and lower boundaries of the OMZ (dissolved oxygen < 0.5 ml l^{-1}), and the horizontal dotted lines indicate the minimum oxygen.

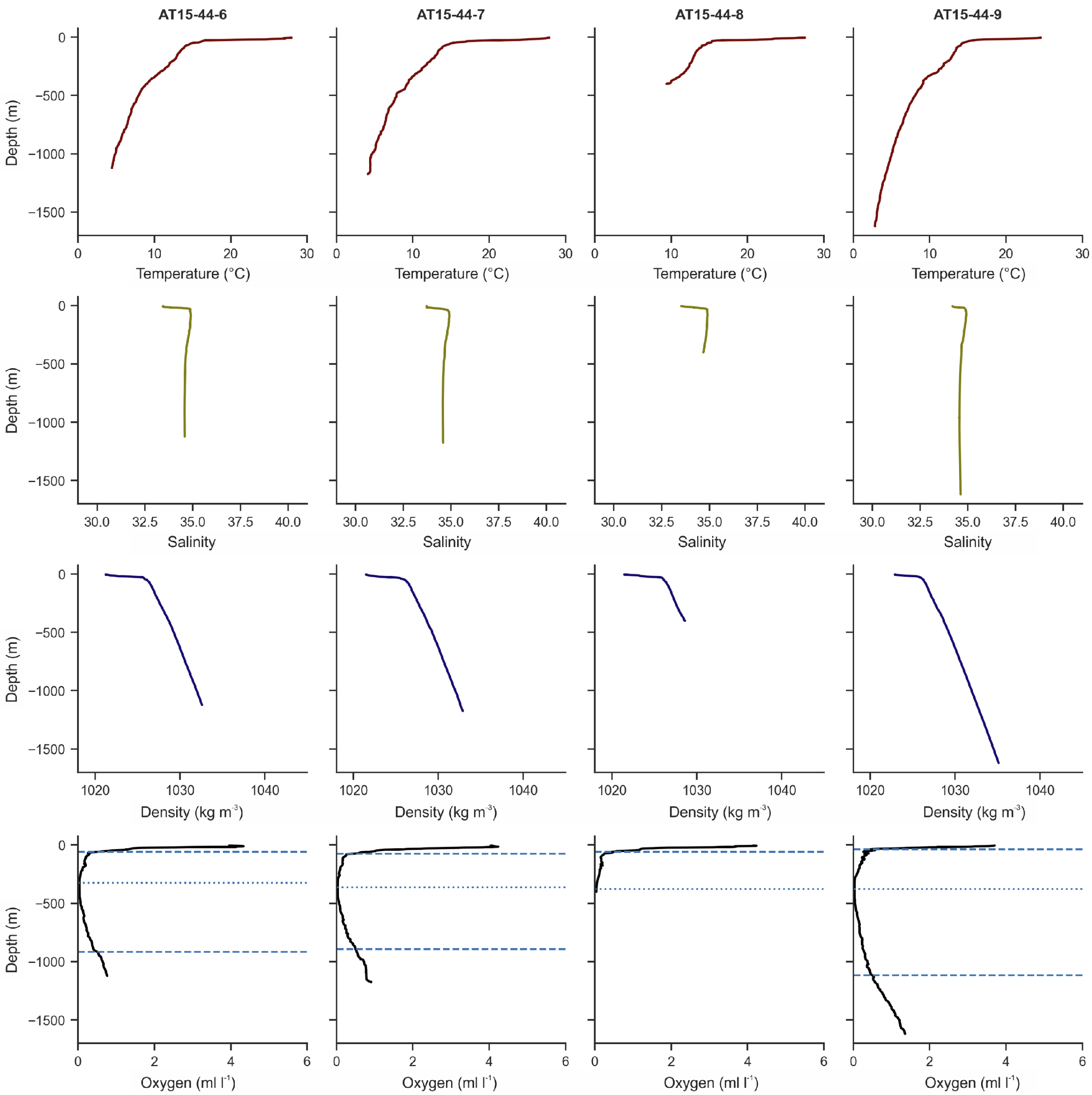

Figure A3. Temperature, salinity, density, and oxygen, at stations 6, 7, 8, and 9, from data measured by the RV 'Atlantis' CTD profiler during the AT15-44 campaign. In the oxygen profiles, the horizontal dashed lines represent the upper and lower boundaries of the OMZ (dissolved oxygen < 0.5 ml l^{-1}), and the horizontal dotted lines indicate the minimum oxygen.

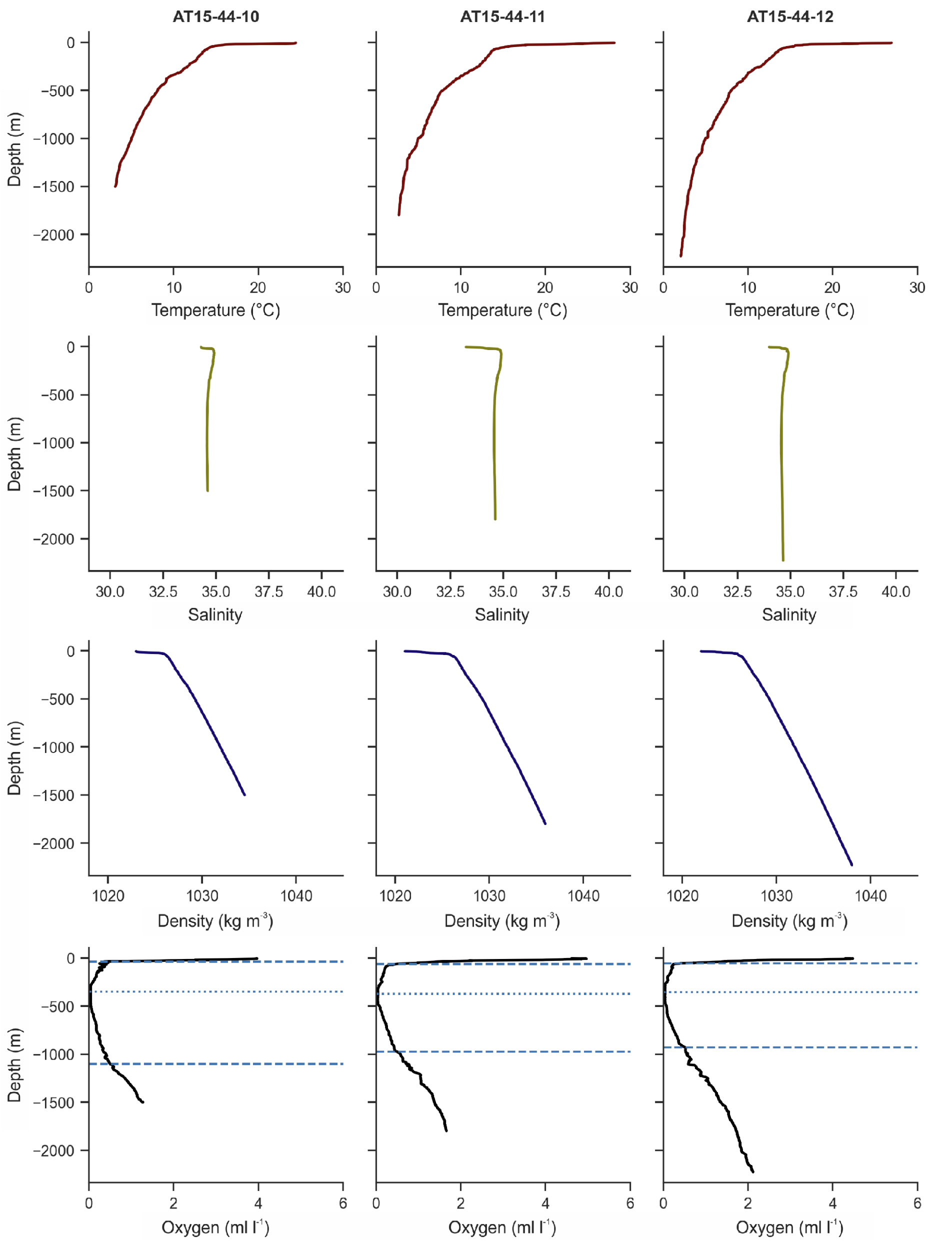

Figure A4. Temperature, salinity, density, and oxygen, at stations 10, 11, and 12, from data measured by the RV 'Atlantis' CTD profiler during the AT15-44 campaign. In the oxygen profiles, the horizontal dashed lines represent the upper and lower boundaries of the OMZ (dissolved oxygen < 0.5 ml l^{-1}), and the horizontal dotted lines indicate the minimum oxygen.

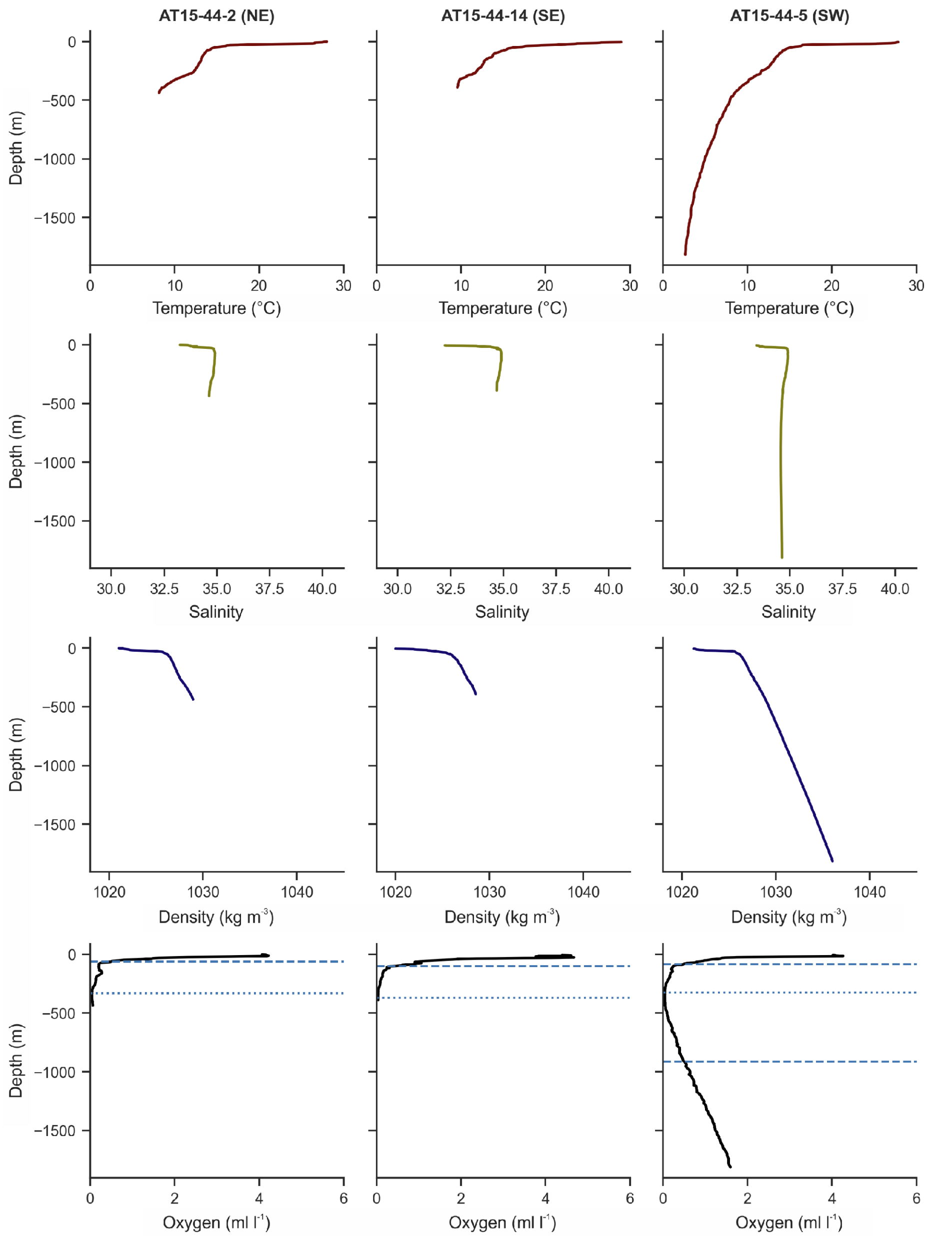

Figure A5. Temperature, salinity, density, and oxygen, at stations 2 (NE), 14 (SE), and 5 (SW), from data measured by the RV 'Atlantis' CTD profiler during the AT15-44 campaign. In the oxygen profiles, the horizontal dashed lines represent the upper and lower boundaries of the OMZ (dissolved oxygen < 0.5 ml l^{-1}), and the horizontal dotted lines indicate the minimum oxygen.

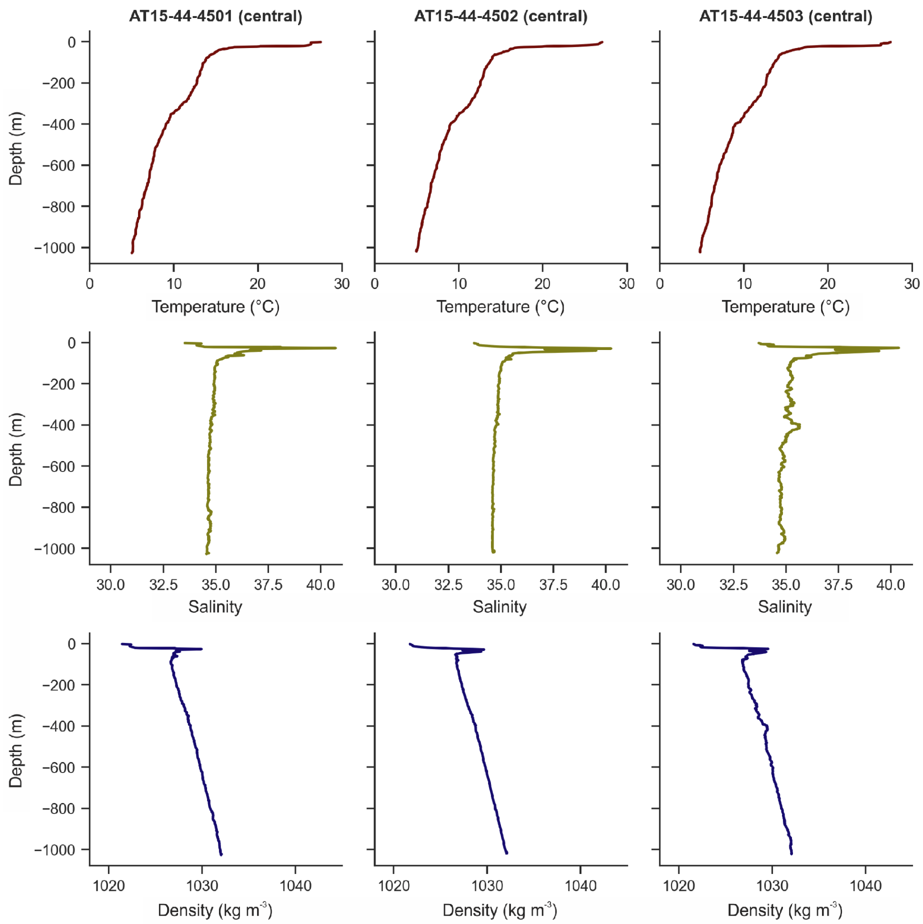

Figure A6. Temperature, salinity, and density, at stations 4501, 4502, and 4503 (Central), from data measured by the HOV 'Alvin' CTD profiler during the AT15-44 campaign.

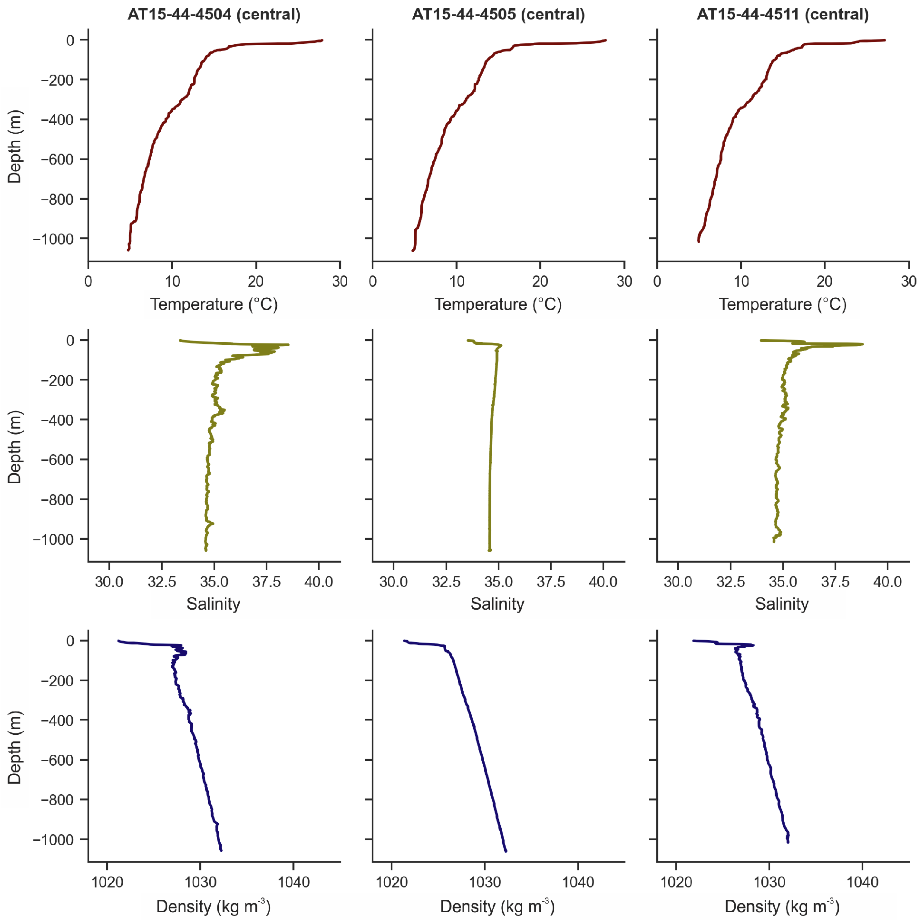

Figure A7. Temperature, salinity, and density, at stations 4504, 4505, and 4511 (Central), from data measured by the HOV 'Alvin' CTD profiler during the AT15-44 campaign.

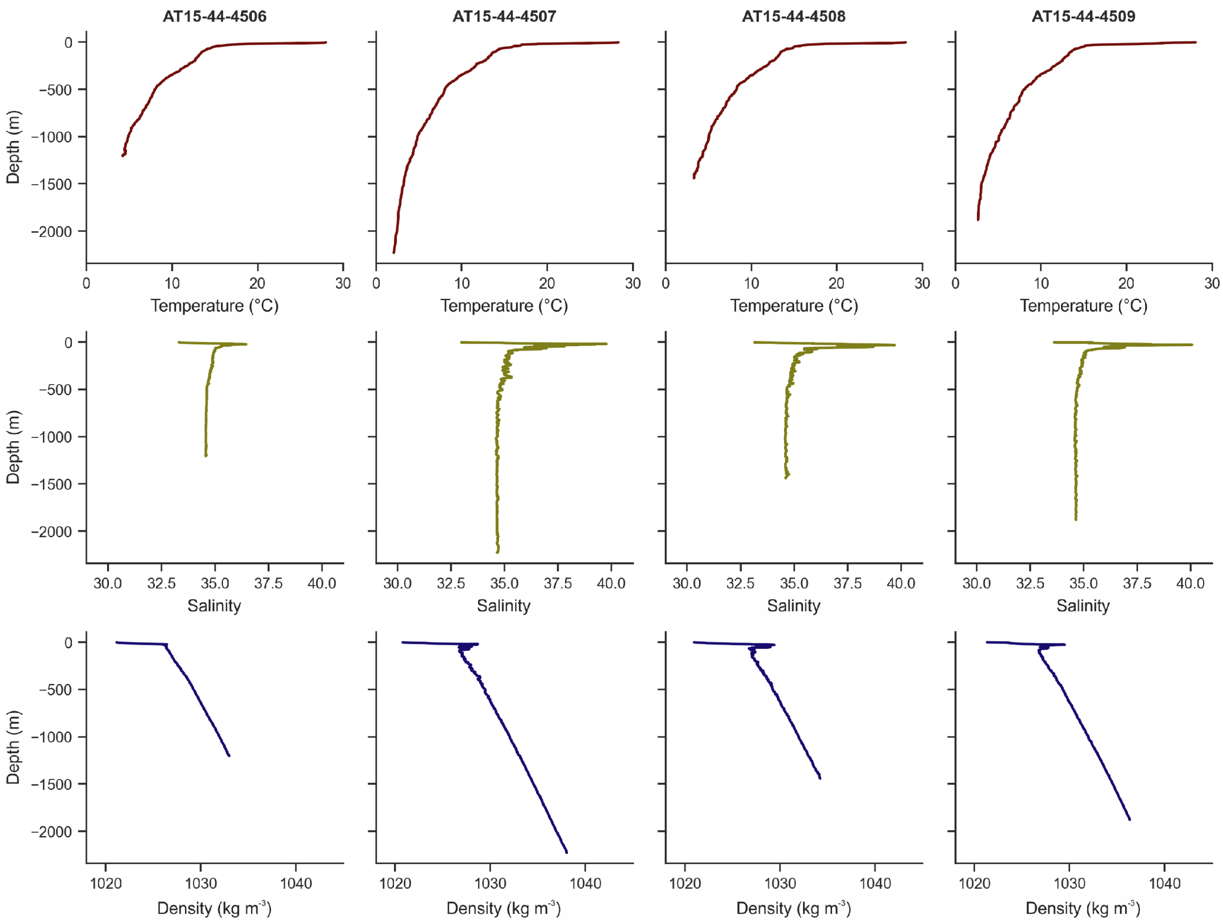

Figure A8. Temperature, salinity, and density, at stations 4506, 4507, 4508, and 4509, from data measured by the HOV 'Alvin' CTD profiler during the AT15-44 campaign.

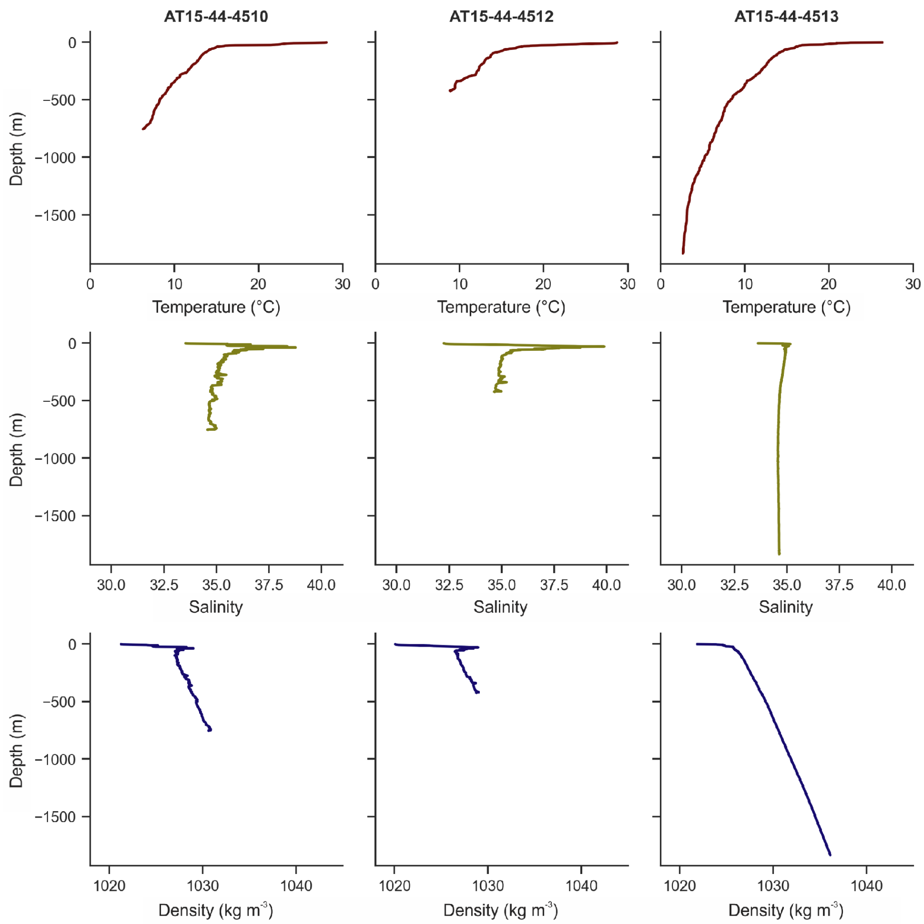

Figure A9. Temperature, salinity, and density, at stations 4510, 4512, and 4513, from data measured by the HOV 'Alvin' CTD profiler during the AT15-44 campaign.

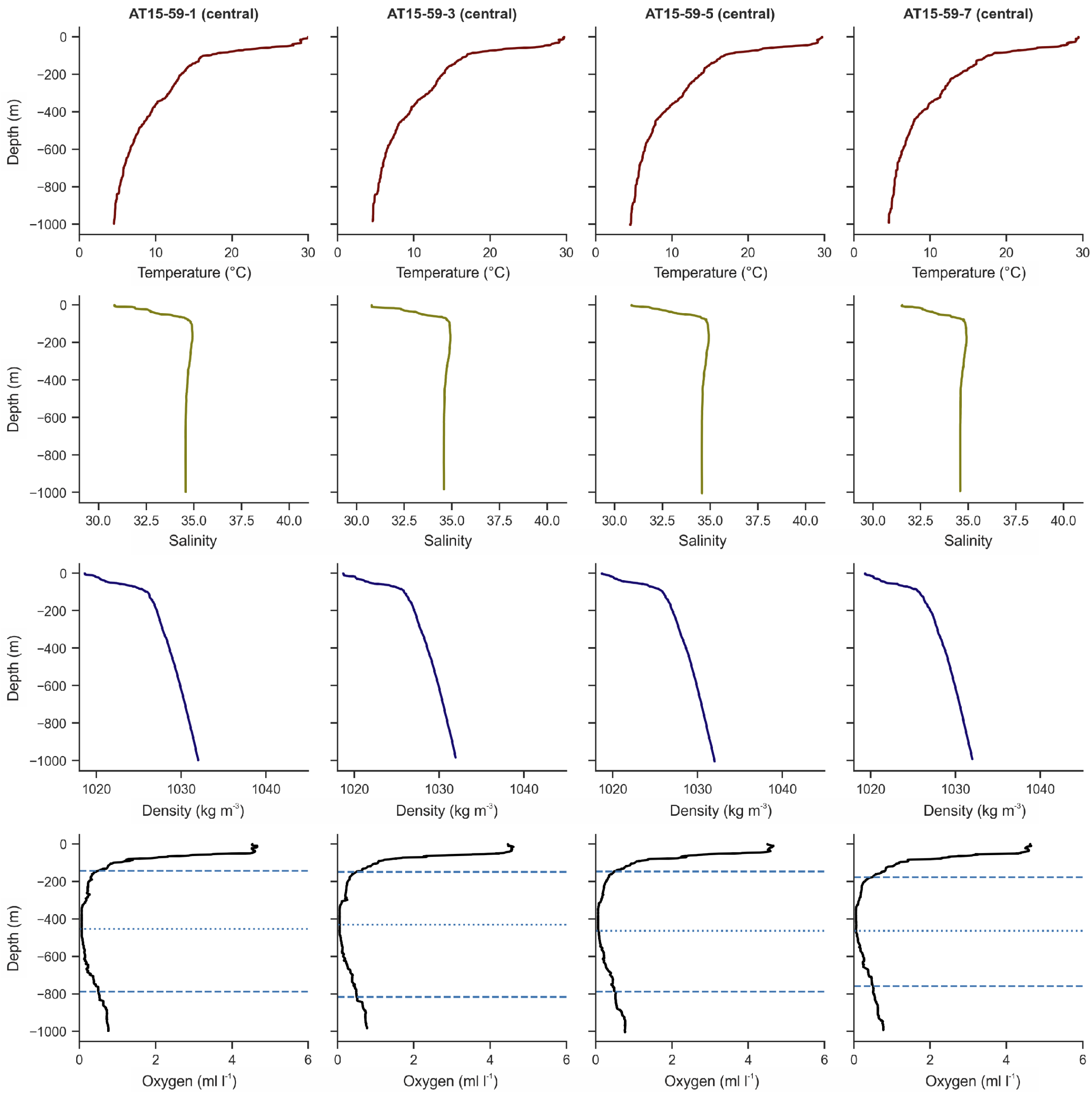

Figure A10. Temperature, salinity, density, and oxygen, at stations 1, 3, 5, and 7 (Central), from data measured by the RV 'Atlantis' CTD profiler during the AT15-59 campaign. In the oxygen profiles, the horizontal dashed lines represent the upper and lower boundaries of the OMZ (dissolved oxygen < 0.5 ml l^{-1}), and the horizontal dotted lines indicate the minimum oxygen.

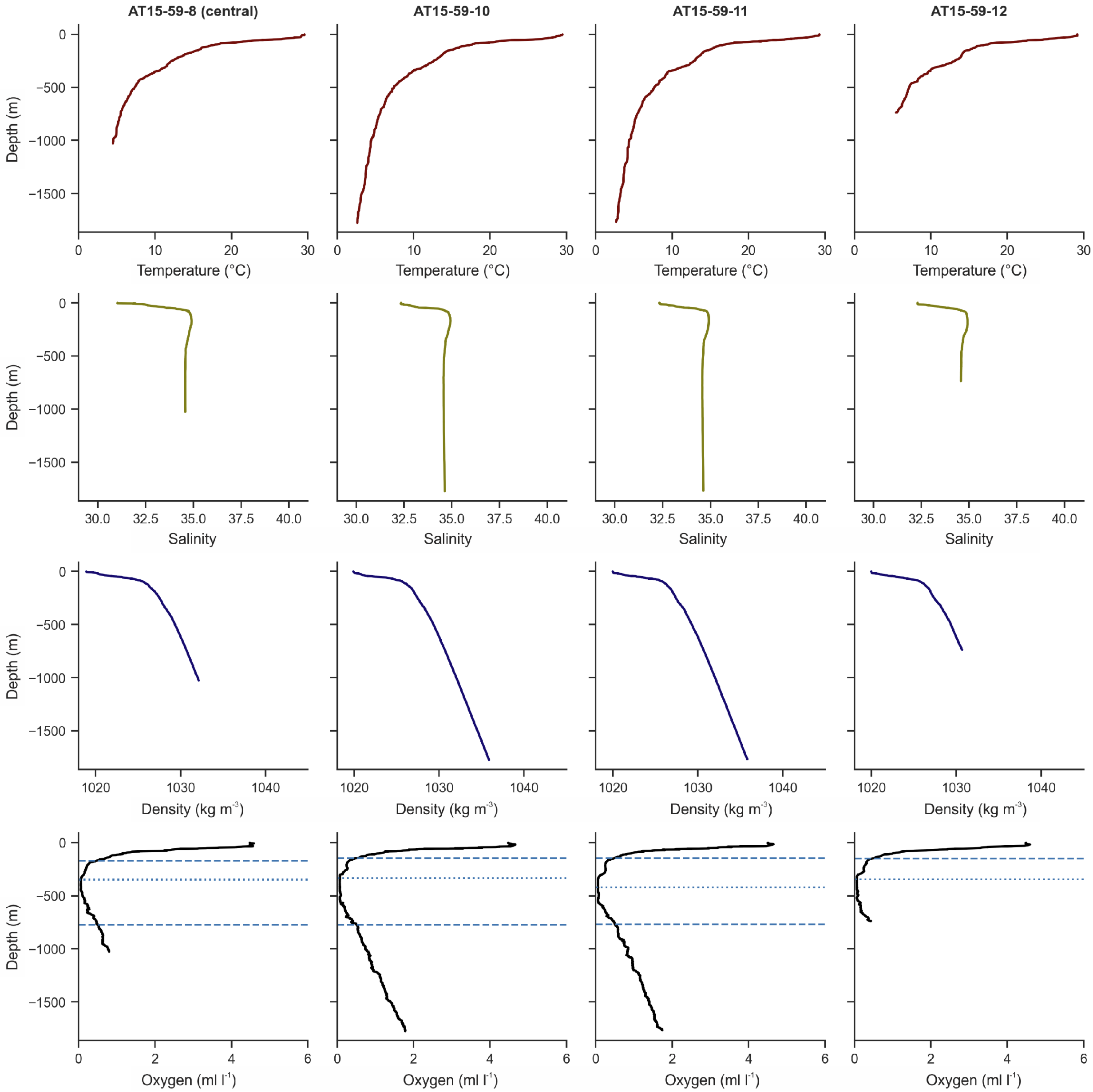

Figure A11. Temperature, salinity, density, and oxygen, at stations 8 (Central), and stations 10, 11, and 12, from data measured by the RV 'Atlantis' CTD profiler during the AT15-59 campaign. In the oxygen profiles, the horizontal dashed lines represent the upper and lower boundaries of the OMZ (dissolved oxygen < 0.5 ml l^{-1}), and the horizontal dotted lines indicate the minimum oxygen.

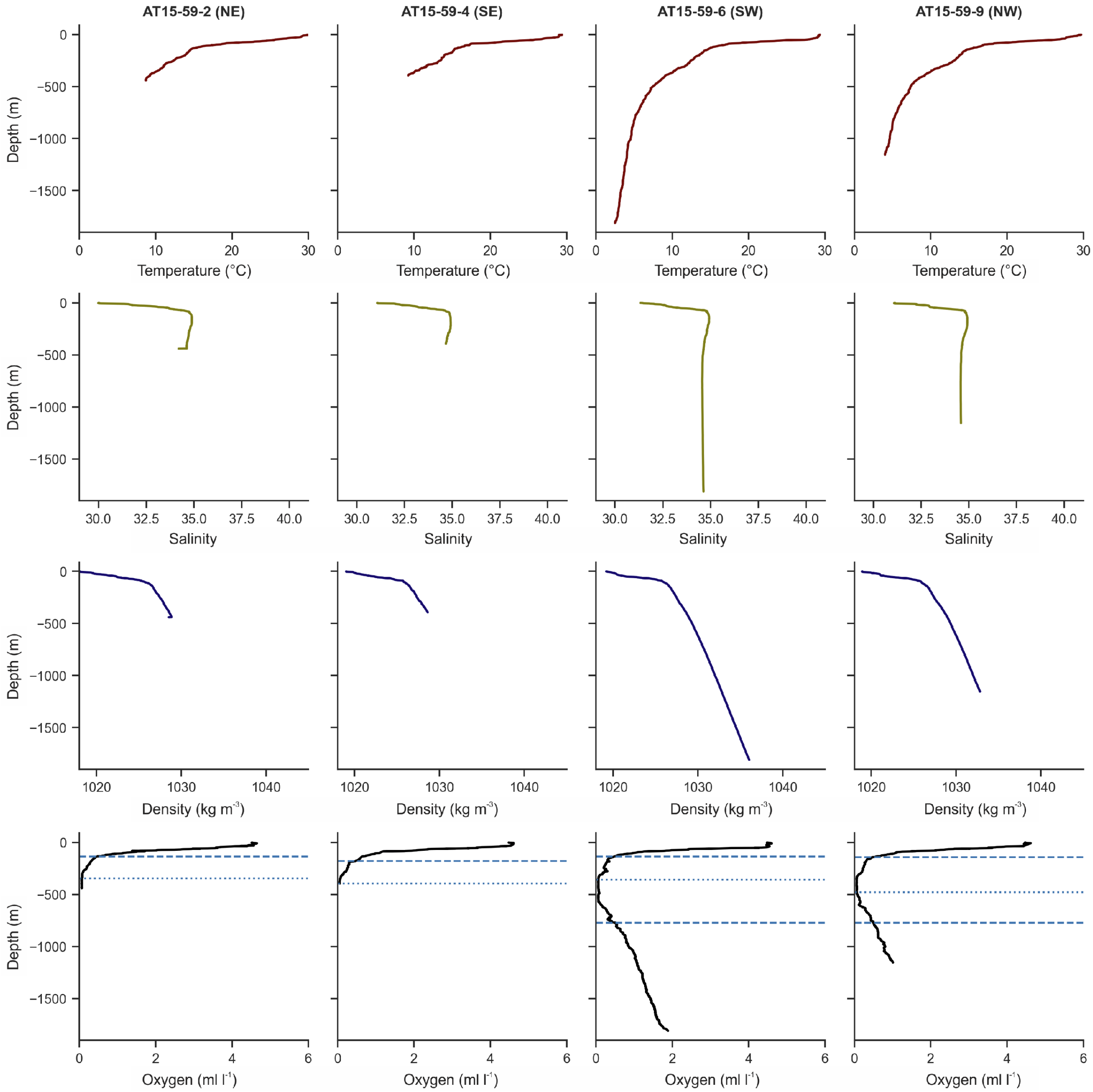

Figure A12. Temperature, salinity, density, and oxygen, at stations 2 (NE), 4 (SE), 6 (SW), and 9 (NW), from data measured by the RV 'Atlantis' CTD profiler during the AT15-59 campaign. In the oxygen profiles, the horizontal dashed lines represent the upper and lower boundaries of the OMZ (dissolved oxygen < 0.5 ml l^{-1}), and the horizontal dotted lines indicate the minimum oxygen.

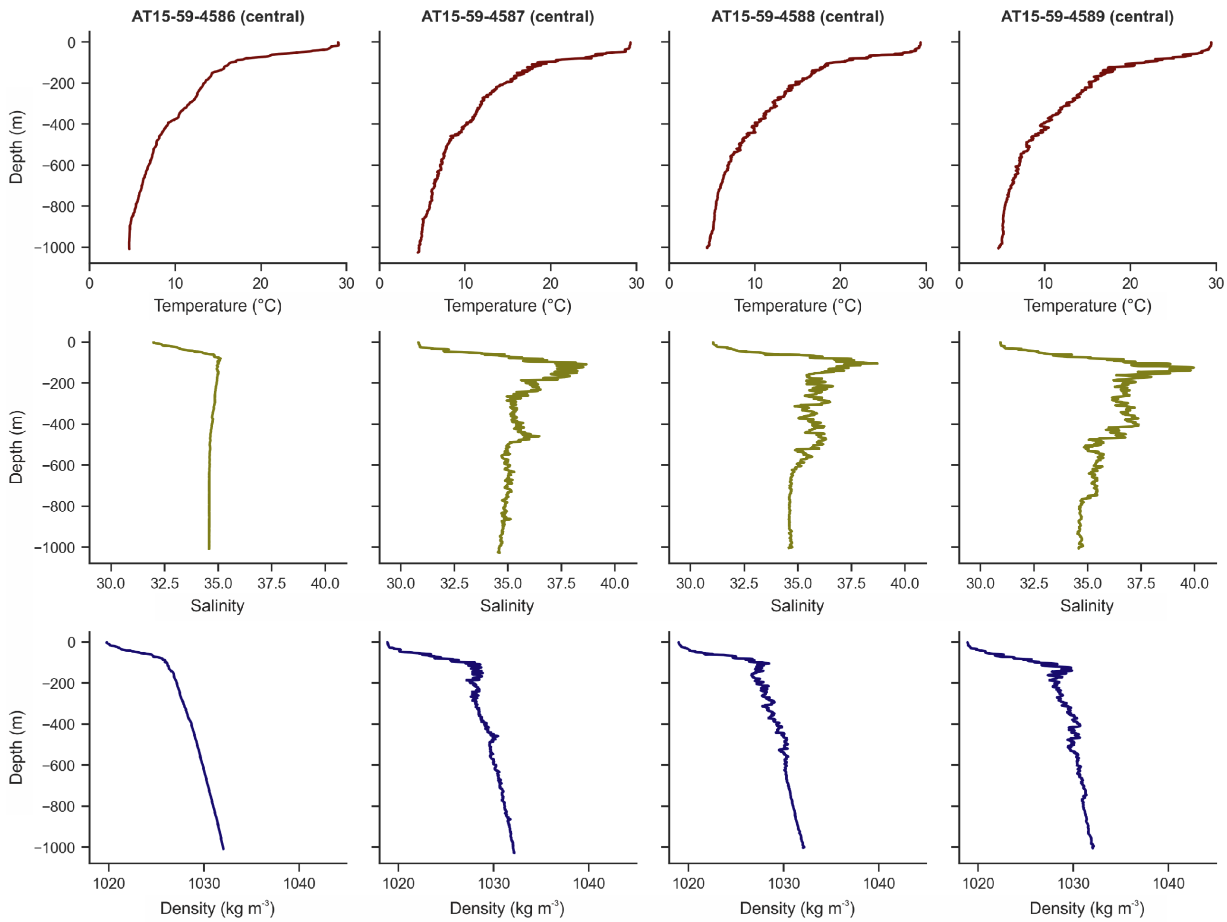

Figure A13. Temperature, salinity, and density, at stations 4586, 4587, 4588, and 4589 (Central), from data measured by the HOV 'Alvin' CTD profiler during the AT15-59 campaign.

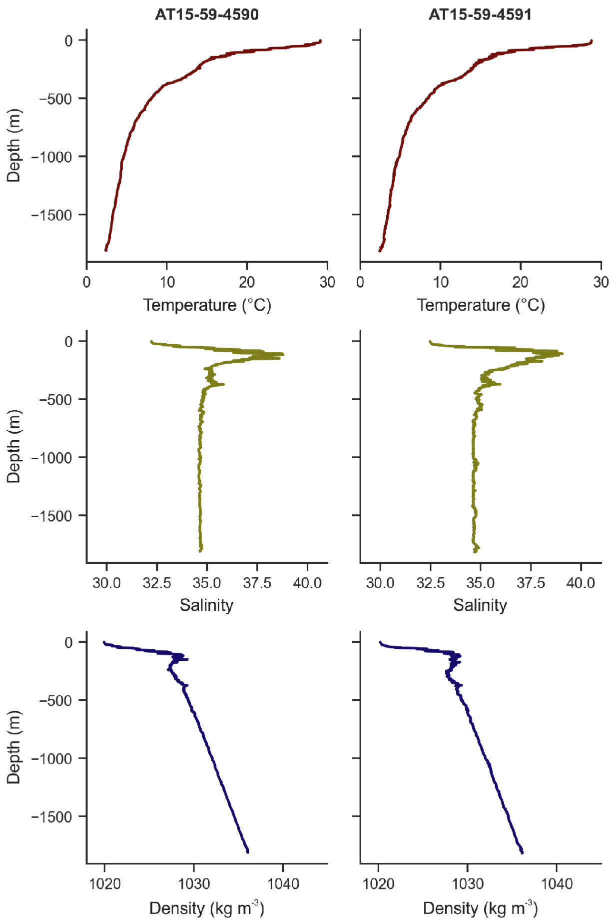

Figure A14. Temperature, salinity, and density, at stations 4590 and 4591, from data measured by the HOV 'Alvin' CTD profiler during the AT15-59 campaign.

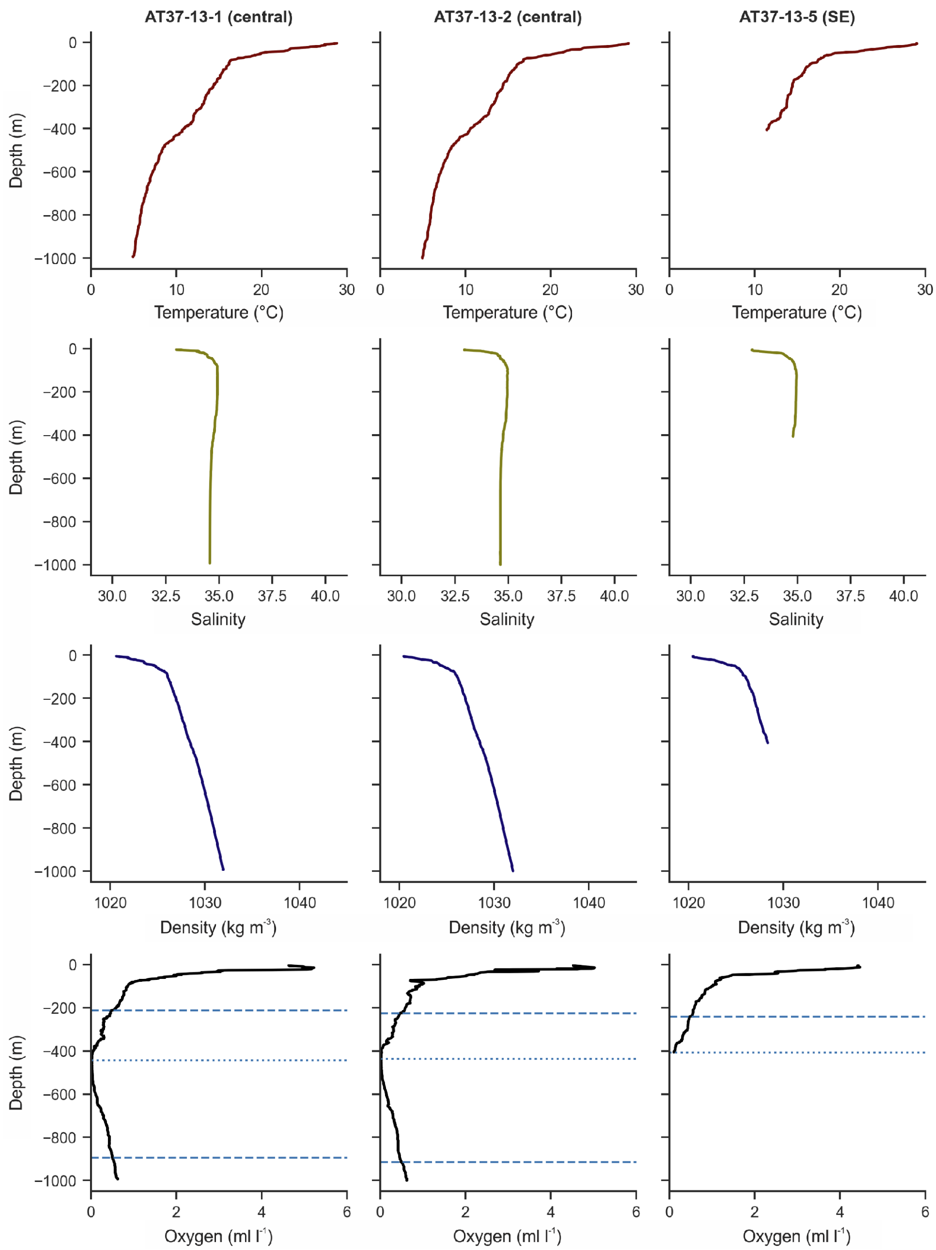

Figure A15. Temperature, salinity, density, and oxygen, at stations 1 and 2 (Central), and station 5 (SE), from data measured by the RV 'Atlantis' CTD profiler during the AT37-13 campaign. In the oxygen profiles, the horizontal dashed lines represent the upper and lower boundaries of the OMZ (dissolved oxygen < 0.5 ml l^{-1}), and the horizontal dotted lines indicate the minimum oxygen.

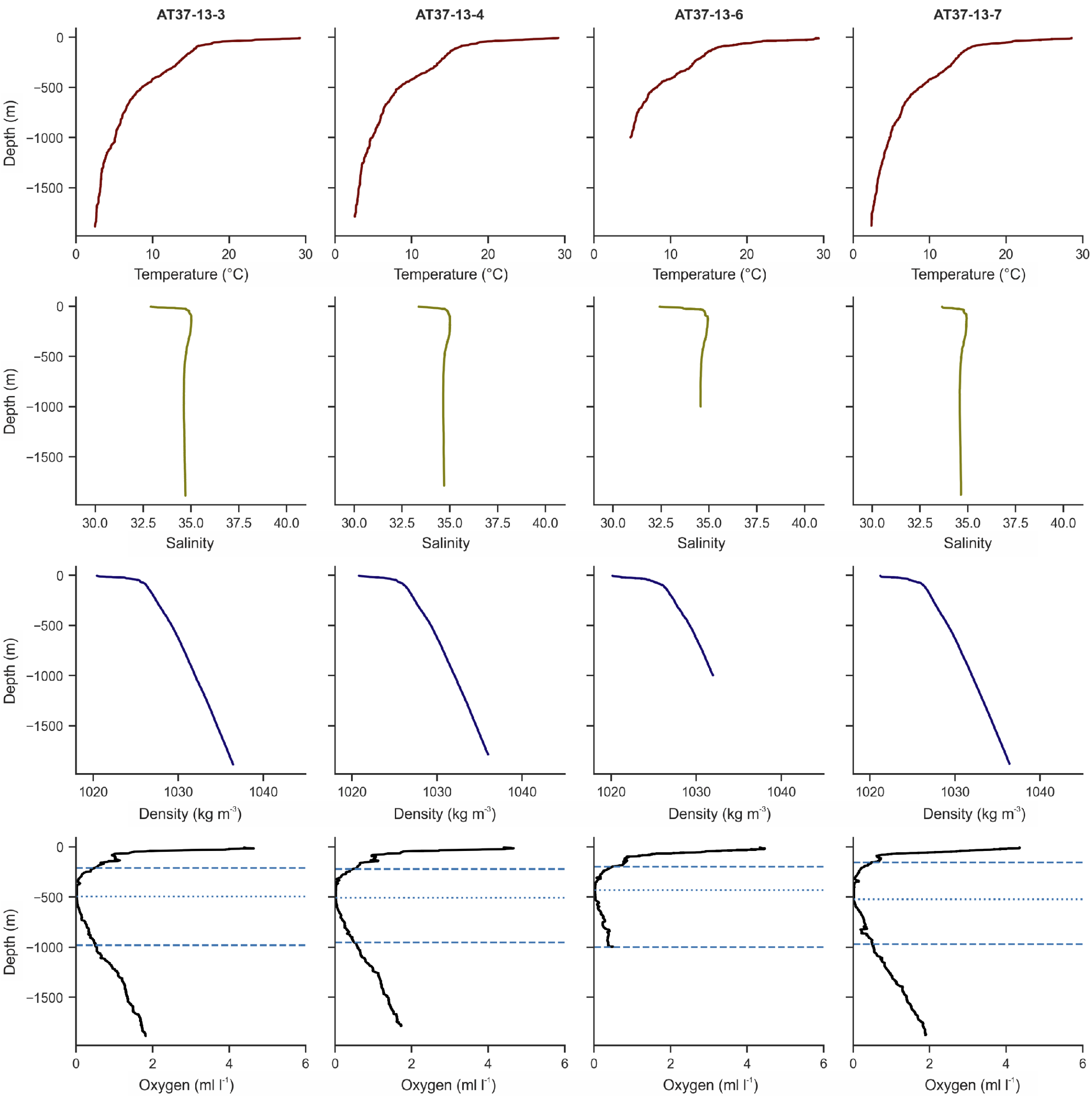

Figure A16. Temperature, salinity, density, and oxygen, at stations 3, 4, 6, and 7, from data measured by the RV 'Atlantis' CTD profiler during the AT37-13 campaign. In the oxygen profiles, the horizontal dashed lines represent the upper and lower boundaries of the OMZ (dissolved oxygen < 0.5 ml l^{-1}), and the horizontal dotted lines indicate the minimum oxygen.

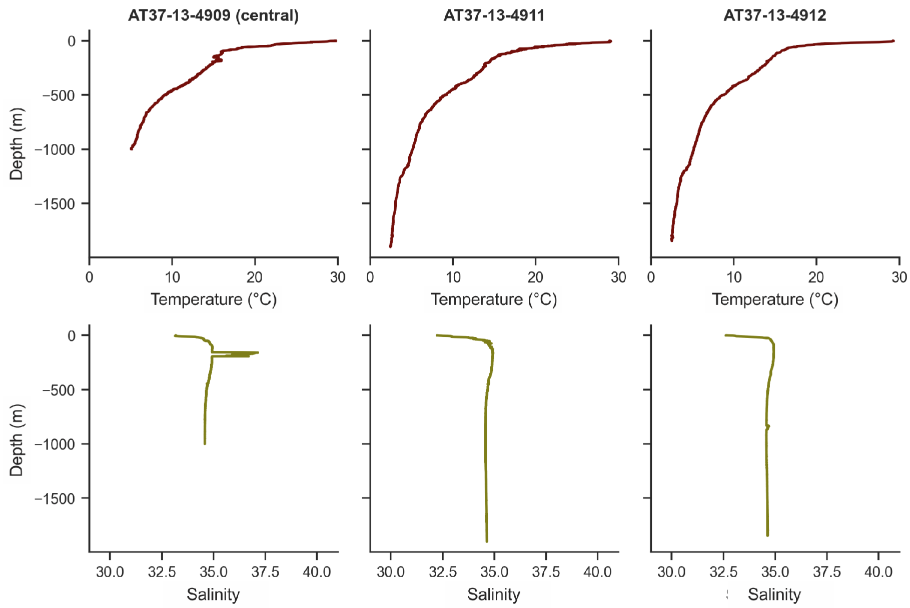

Figure A17. Temperature and salinity, at station 4909 (Central), and stations 4911 and 4912, from data measured by the HOV 'Alvin' CTD profiler during the AT37-13 campaign.

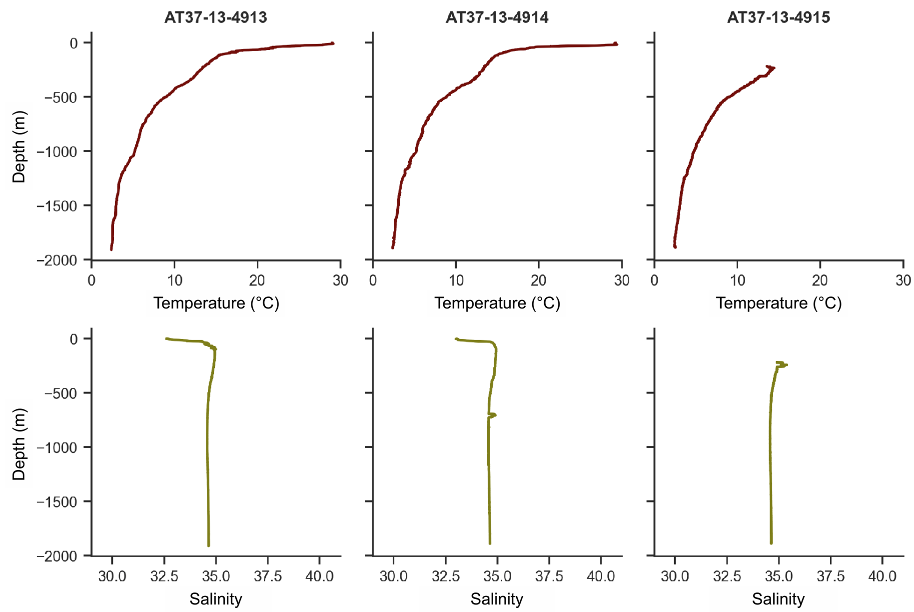

Figure A18. Temperature and salinity, at stations 4913, 4914, and 4915, from data measured by the HOV 'Alvin' CTD profiler during the AT37-13 campaign.